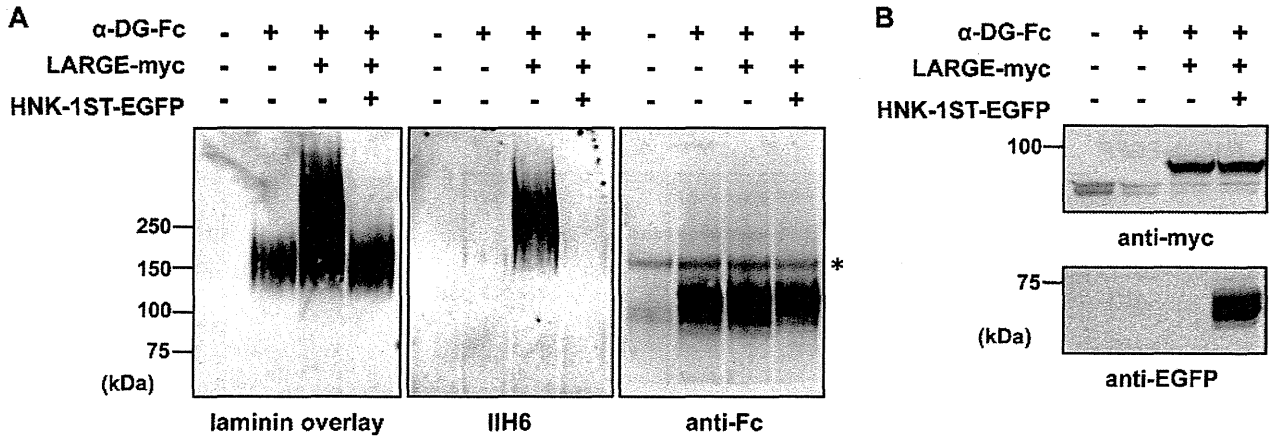

FIGURE 3. **Influence of HNK-1ST on the glycosylation and function of α-DG.** *A*, α-DG-Fc, LARGE-myc, and HNK-1ST-EGFP were transiently co-expressed in CHO-K1 cells as shown. α-DG-Fc was pulled down from the culture medium and assayed for laminin binding activity by the ligand overlay assay and for glycosylation by Western blotting with IIH6 mAb. Anti-Fc pAb was used to confirm equal protein loading. * indicates nonspecific bands. *B*, CHO-K1 cell lysates were analyzed by Western blotting using anti-Myc and anti-EGFP mAbs to assess the expression of LARGE-myc and HNK-1ST-EGFP.

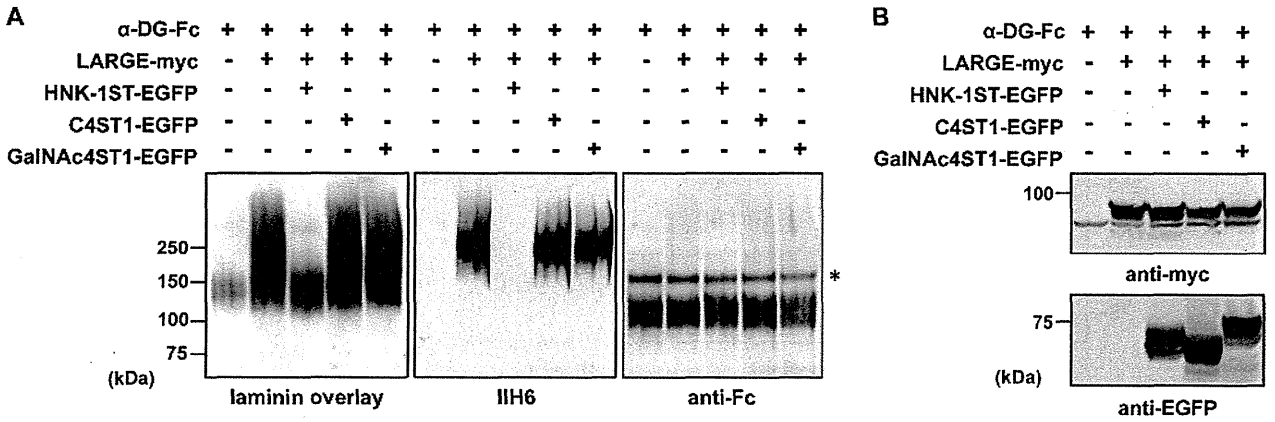

FIGURE 4. **Effect of other sulfotransferases on the glycosylation of α-DG.** *A*, CHO-K1 cells were co-transfected with α-DG-Fc, LARGE-myc, and various EGFP-fused sulfotransferases belonging to the HNK-1ST family as indicated. α-DG-Fc was pulled down from the culture medium and analyzed by laminin overlay assay and Western blotting with IIH6 mAb and anti-Fc pAb. * indicates nonspecific bands. *B*, expression of LARGE-myc and sulfotransferases was confirmed by Western blotting of cell lysates using anti-Myc mAb and anti-EGFP mAb.

DISCUSSION

Melanoma is one of the most malignant tumors, showing high metastatic ability and a rapid progression, which leads to a poor prognosis. Expression of the HNK-1 epitope is found in both primary and metastatic lesions in cases of melanoma (45, 46) and correlates with metastatic behavior (46). In addition, the HNK-1 carbohydrate positively affects the invasive and adhesive functions of melanoma cells, demonstrating the relationship between HNK-1 expression and the aggressiveness of melanomas (47). Meanwhile, HNK-1ST, one of the enzymes producing the HNK-1 carbohydrate, was identified as a candidate suppressor for melanoma invasiveness by Zhao *et al.* (6). Apparent confounding issues are that HNK-1ST functions as a tumor suppressor, although the resulting product, the HNK-1 epitope, promotes metastasis. However, it should be noted that whereas Zhao *et al.* (6) reported that HNK-1ST functions as a tumor suppressor, they failed to detect the HNK-1 epitope in 56 primary and 20 metastatic melanomas. This means that HNK-1ST might regulate invasiveness through an HNK-1 epitope-independent pathway. As a possible solution to this problem, our findings revealed that α-DG-dependent migration is another mechanism of metastasis independent of the HNK-1 epitope. Furthermore, we disclosed here a novel role of HNK-1ST, the functional regulation of α-DG via post-translational modification. This distinct function of HNK-1ST does not require GlcAT-P and GlcAT-S (Fig. 3), which accounts for the absence of the HNK-1 epitope despite the expression of HNK-1ST. Moreover, HNK-1 is not constantly expressed in melanoma lesions or cell lines (45–47), indicating that there are at least two subpopulations of melanomas, *i.e.* HNK-1-positive and -negative. Hence, α-DG-dependent migration controlled by HNK-1ST might predominate in HNK-1-negative melanomas. The unique glycan structure expressed on α-DG has been shown to have a close relationship to tumor-related phenotypes such as invasiveness (32, 33). Previous studies reported that the IIH6 mAb-reactive glycan of α-DG had a suppressive effect on tumor invasion in cases of breast, prostate, and lung carcinoma (32, 33), although we obtained the opposite results using melanoma cells (Figs. 1 and 2), suggesting that the role of α-DG varies depending on the type of cancer. Therefore, we found that

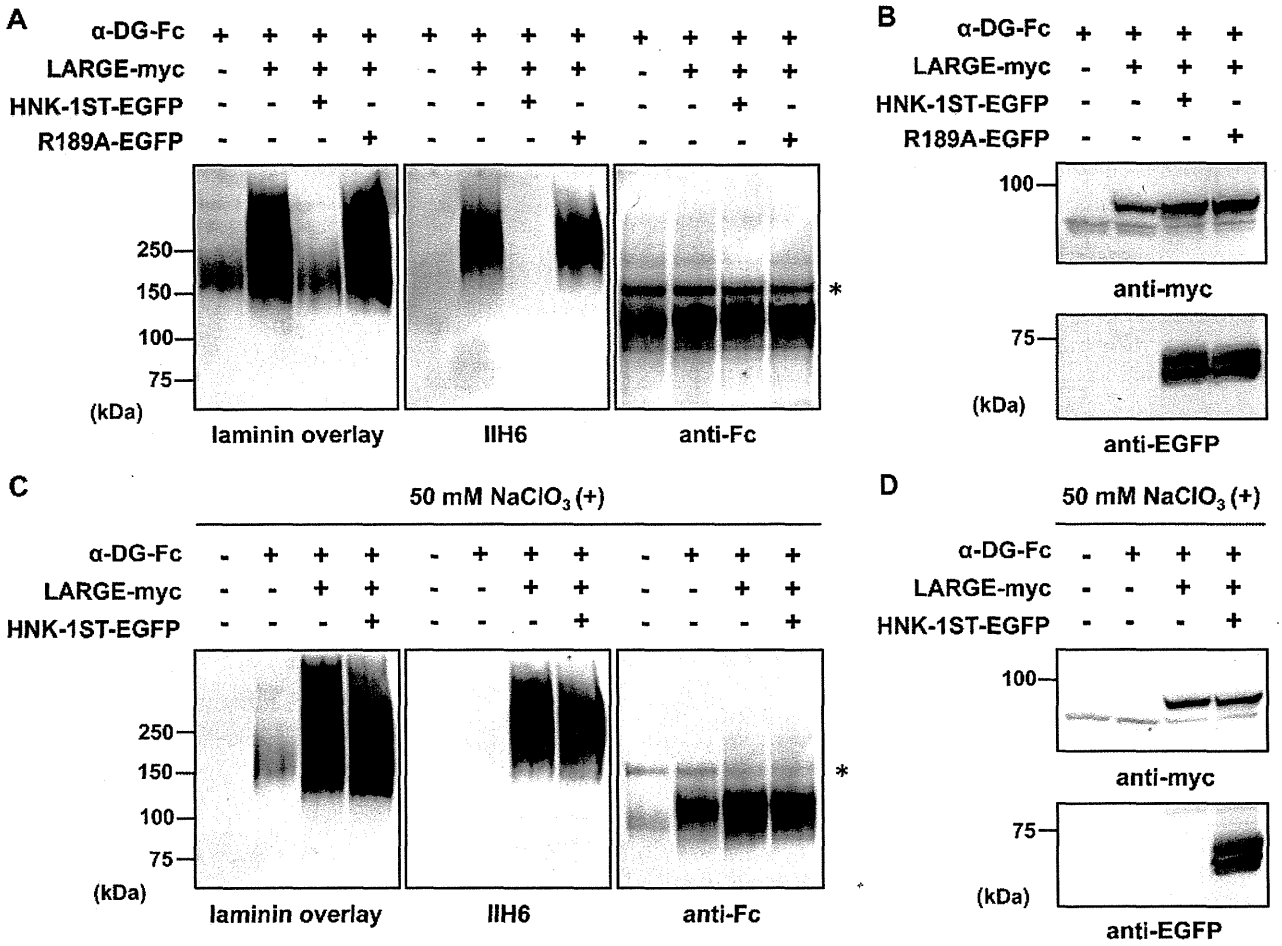

FIGURE 5. **Importance of sulfotransferase activity of HNK-1ST to the α-DG-modulating function.** *A* and *B*, requirement of the sulfotransferase activity was investigated using an activity-abolished mutant of HNK-1ST (R189A-EGFP). *A*, α-DG-Fc, LARGE-myc, and wild-type or R189A HNK-1ST-EGFP were transiently co-expressed in CHO-K1 cells as shown. α-DG-Fc was precipitated from the culture medium and analyzed by laminin overlay assay and Western blotting with IIH6 mAb and anti-Fc pAb. * indicates nonspecific bands. *B*, cell lysates were subjected to Western blotting using anti-Myc and anti-EGFP mAbs to assess the expression of LARGE-myc and wild-type or R189A HNK-1ST-EGFP. *C* and *D*, importance of the sulfotransferase activity was examined by PAPS inhibition experiments using sodium chlorate ($NaClO_3$). *C*, CHO-K1 cells were transiently transfected with α-DG-Fc, LARGE-myc, and HNK-1ST-EGFP in combination as indicated and then treated with $NaClO_3$ for 48 h. α-DG-Fc was precipitated from the culture medium and analyzed by laminin overlay assay and Western blotting with IIH6 mAb and anti-Fc pAb. * indicates nonspecific bands. *D*, expression of LARGE-myc and HNK-1ST-EGFP was confirmed by Western blotting of CHO-K1 cell lysates using anti-Myc and anti-EGFP mAbs.

HNK-1ST has a potential role modulating invasiveness by controlling the glycosylation of α-DG, leading to tumor suppression in melanoma cases.

Of particular interest was that overexpression or RA-mediated up-regulation of HNK-1ST did not completely abolish the laminin binding activity of α-DG in S91 and CHO-K1 cells, although IIH6 immunoreactivity disappeared in the same samples (Figs. 1–5). This suggests that sulfation by HNK-1ST evokes inhibitory effects predominantly on the IIH6 mAb-reactive glycan among the heterogeneous carbohydrate structures of α-DG, resulting in substantial laminin binding activity of α-DG remaining. The IIH6-reactive epitope and laminin-binding glycan are known to somewhat overlap (23). However, whether these two moieties are identical or not is still unclear despite a number of structural analyses on the glycosylation of α-DG (48–50). Chiba *et al.* (51) reported that a unique *O*-mannosyltetrasaccharide on α-DG has the ability to bind to laminin. More recently, a novel phosphate-containing glycan was identified on α-DG (52). The phosphate is attached to the 6-*O*-position of *O*-linked mannose, and post-phosphoryl glycosylation mediated by LARGE is essential for α-DG-ligand interaction and IIH6 epitope production (52). We demonstrated that LARGE could not generate the IIH6 epitope on α-DG in the presence of HNK-1ST (Figs. 3–5) and HNK-1ST indeed transferred a sulfate group onto α-DG (Fig. 6*B*), suggesting that HNK-1ST inhibits the LARGE-dependent post-phosphoryl modification of α-DG by sulfate transfer. Therefore, identification of the specific site of α-DG sulfated by HNK-1ST and the structure of the resulting sulfated glycan might be important for elucidating LARGE-dependent glycosylation.

During the preparation of this manuscript, Campbell and co-workers (53) reported that LARGE could act as a bifunctional glycosyltransferase with both xylosyl- and glucuronyltransferase activities and could generate a linear polysaccharide structure composed of repeating disaccharide units (-3-xylose-α1,3-GlcAβ1-) on α-DG. HNK-1ST has the ability to transfer a

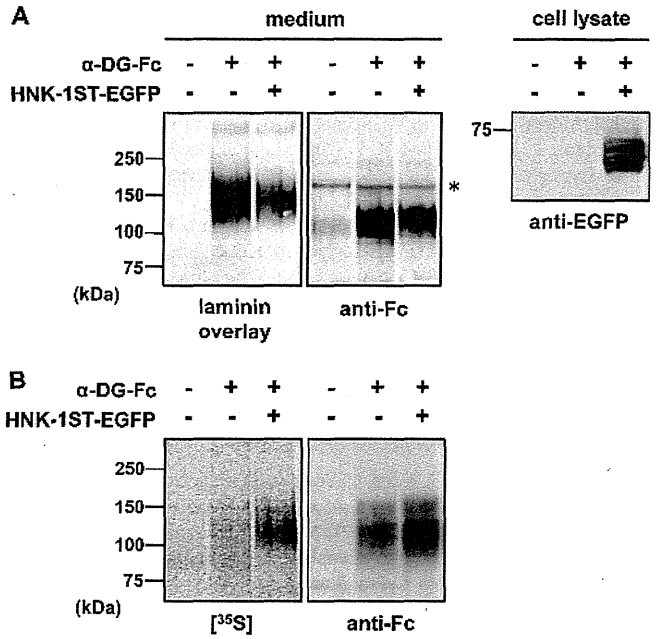

FIGURE 6. **HNK-1ST-mediated incorporation of sulfate into α-DG.** *A*, α-DG-Fc and HNK-1ST-EGFP were transiently expressed in CHO-K1 cells as shown. α-DG-Fc was pulled down from the cultured medium and analyzed by laminin overlay assay and Western blotting with anti-Fc pAb (*medium*). The cell lysates were subjected to Western blotting using anti-EGFP mAb to assess the expression of HNK-1ST-EGFP (*cell lysate*). * indicates nonspecific bands. *B*, CHO-K1 cells transiently expressing α-DG-Fc with (+) or without (−) HNK-1ST-EGFP were labeled with radioactive [^{35}S]sodium sulfate. α-DG-Fc was pulled down from the culture medium, separated by SDS-PAGE, and subjected to autoradiography and Western blotting with anti-Fc.

sulfate group to the C-3 position of terminal GlcA, where xylose is transferred; therefore, it makes sense that HNK-1ST inhibits IIH6-reactive glycan produced by LARGE. Our data presented in this study are highly important for understanding dystroglycan function via its glycosylation.

In mammals, an apparent molecular mass of α-DG varies from highly limited (about 120 kDa, *e.g.* brain) to rather broad (120–200 kDa, *e.g.* muscle) due to its glycosylation in a tissue-dependent manner (18, 19, 21). In contrast, in experiments using cell lines, forced expression of LARGE always yields an extensively glycosylated α-DG that appears as a band of ≥200 kDa on SDS-PAGE (Figs. 2–5) (37, 38, 41), implying the presence of an unidentified machinery that negatively regulates the glycosylation of α-DG *in vivo*. Hence, we propose HNK-1ST to be one such suppressive factor for α-DG function, acting as a "molecular brake" to generate properly glycosylated α-DG. In this regard, future studies might identify a pathogenic mutation of *HNK-1ST* in CMD patients, which causes hyperactivation of HNK-1ST resulting in hypoglycosylation of α-DG. Investigating the α-DG-modulating function of HNK-1ST could be a powerful means of uncovering the regulatory system of α-DG glycosylation, contributing to the development of therapeutic strategies for glycosylation-defective CMDs.

REFERENCES

1. Friedl, P., and Alexander, S. (2011) Cancer invasion and the microenvironment. Plasticity and reciprocity. *Cell* **147,** 992–1009
2. Ohtsubo, K., and Marth, J. D. (2006) Glycosylation in cellular mechanisms of health and disease. *Cell* **126,** 855–867
3. Fuster, M. M., and Esko, J. D. (2005) The sweet and sour of cancer. Glycans as novel therapeutic targets. *Nat. Rev. Cancer* **5,** 526–542
4. Meany, D. L., and Chan, D. W. (2011) Aberrant glycosylation associated with enzymes as cancer biomarkers. *Clin. Proteomics* **8,** 7
5. Hakomori, S. (1996) Tumor malignancy defined by aberrant glycosylation and sphingo(glyco)lipid metabolism. *Cancer Res.* **56,** 5309–5318
6. Zhao, X., Graves, C., Ames, S. J., Fisher, D. E., and Spanjaard, R. A. (2009) Mechanism of regulation and suppression of melanoma invasiveness by novel retinoic acid receptor-γ target gene carbohydrate sulfotransferase 10. *Cancer Res.* **69,** 5218–5225
7. Morita, I., Kizuka, Y., Kakuda, S., and Oka, S. (2008) Expression and function of the HNK-1 carbohydrate. *J. Biochem.* **143,** 719–724
8. Morita, I., Kakuda, S., Takeuchi, Y., Kawasaki, T., and Oka, S. (2009) HNK-1 (human natural killer-1) glyco-epitope is essential for normal spine morphogenesis in developing hippocampal neurons. *Neuroscience* **164,** 1685–1694
9. Morita, I., Kakuda, S., Takeuchi, Y., Itoh, S., Kawasaki, N., Kizuka, Y., Kawasaki, T., and Oka, S. (2009) HNK-1 glyco-epitope regulates the stability of the glutamate receptor subunit GluR2 on the neuronal cell surface. *J. Biol. Chem.* **284,** 30209–30217
10. Yamamoto, S., Oka, S., Inoue, M., Shimuta, M., Manabe, T., Takahashi, H., Miyamoto, M., Asano, M., Sakagami, J., Sudo, K., Iwakura, Y., Ono, K., and Kawasaki, T. (2002) Mice deficient in nervous system-specific carbohydrate epitope HNK-1 exhibit impaired synaptic plasticity and spatial learning. *J. Biol. Chem.* **277,** 27227–27231
11. Chou, D. K., Ilyas, A. A., Evans, J. E., Costello, C., Quarles, R. H., and Jungalwala, F. B. (1986) Structure of sulfated glucuronyl glycolipids in the nervous system reacting with HNK-1 antibody and some IgM paraproteins in neuropathy. *J. Biol. Chem.* **261,** 11717–11725
12. Ariga, T., Kohriyama, T., Freddo, L., Latov, N., Saito, M., Kon, K., Ando, S., Suzuki, M., Hemling, M. E., and Rinehart, K. L., Jr. (1987) Characterization of sulfated glucuronic acid containing glycolipids reacting with IgM M-proteins in patients with neuropathy. *J. Biol. Chem.* **262,** 848–853
13. Kizuka, Y., Matsui, T., Takematsu, H., Kozutsumi, Y., Kawasaki, T., and Oka, S. (2006) Physical and functional association of glucuronyltransferases and sulfotransferase involved in HNK-1 biosynthesis. *J. Biol. Chem.* **281,** 13644–13651
14. Terayama, K., Oka, S., Seiki, T., Miki, Y., Nakamura, A., Kozutsumi, Y., Takio, K., and Kawasaki, T. (1997) Cloning and functional expression of a novel glucuronyltransferase involved in the biosynthesis of the carbohydrate epitope HNK-1. *Proc. Natl. Acad. Sci. U.S.A.* **94,** 6093–6098
15. Seiki, T., Oka, S., Terayama, K., Imiya, K., and Kawasaki, T. (1999) Molecular cloning and expression of a second glucuronyltransferase involved in the biosynthesis of the HNK-1 carbohydrate epitope. *Biochem. Biophys. Res. Commun.* **255,** 182–187
16. Ong, E., Yeh, J. C., Ding, Y., Hindsgaul, O., and Fukuda, M. (1998) Expression cloning of a human sulfotransferase that directs the synthesis of the HNK-1 glycan on the neural cell adhesion molecule and glycolipids. *J. Biol. Chem.* **273,** 5190–5195
17. Tagawa, H., Kizuka, Y., Ikeda, T., Itoh, S., Kawasaki, N., Kurihara, H., Onozato, M. L., Tojo, A., Sakai, T., Kawasaki, T., and Oka, S. (2005) A nonsulfated form of the HNK-1 carbohydrate is expressed in mouse kidney. *J. Biol. Chem.* **280,** 23876–23883
18. Ibraghimov-Beskrovnaya, O., Ervasti, J. M., Leveille, C. J., Slaughter, C. A., Sernett, S. W., and Campbell, K. P. (1992) Primary structure of dystrophin-associated glycoproteins linking dystrophin to the extracellular matrix. *Nature* **355,** 696–702
19. Barresi, R., and Campbell, K. P. (2006) Dystroglycan. From biosynthesis to pathogenesis of human disease. *J. Cell Sci.* **119,** 199–207
20. Han, R., Kanagawa, M., Yoshida-Moriguchi, T., Rader, E. P., Ng, R. A., Michele, D. E., Muirhead, D. E., Kunz, S., Moore, S. A., Iannaccone, S. T., Miyake, K., McNeil, P. L., Mayer, U., Oldstone, M. B., Faulkner, J. A., and Campbell, K. P. (2009) Basal lamina strengthens cell membrane integrity via the laminin G domain-binding motif of α-dystroglycan. *Proc. Natl. Acad. Sci. U.S.A.* **106,** 12573–12579
21. Ervasti, J. M., Burwell, A. L., and Geissler, A. L. (1997) Tissue-specific heterogeneity in α-dystroglycan sialoglycosylation. Skeletal muscle α-dystroglycan is a latent receptor for *Vicia villosa* agglutinin b4 masked by

sialic acid modification. *J. Biol. Chem.* **272,** 22315–22321
22. Michele, D. E., and Campbell, K. P. (2003) Dystrophin-glycoprotein complex. Post-translational processing and dystroglycan function. *J. Biol. Chem.* **278,** 15457–15460
23. Ervasti, J. M., and Campbell, K. P. (1993) A role for the dystrophin-glycoprotein complex as a transmembrane linker between laminin and actin. *J. Cell Biol.* **122,** 809–823
24. Michele, D. E., Barresi, R., Kanagawa, M., Saito, F., Cohn, R. D., Satz, J. S., Dollar, J., Nishino, I., Kelley, R. I., Somer, H., Straub, V., Mathews, K. D., Moore, S. A., and Campbell, K. P. (2002) Post-translational disruption of dystroglycan-ligand interactions in congenital muscular dystrophies. *Nature* **418,** 417–422
25. Muntoni, F., Torelli, S., and Brockington, M. (2008) Muscular dystrophies due to glycosylation defects. *Neurotherapeutics* **5,** 627–632
26. Beltrán-Valero de Bernabé, D., Currier, S., Steinbrecher, A., Celli, J., van Beusekom, E., van der Zwaag, B., Kayserili, H., Merlini, L., Chitayat, D., Dobyns, W. B., Cormand, B., Lehesjoki, A. E., Cruces, J., Voit, T., Walsh, C. A., van Bokhoven, H., and Brunner, H. G. (2002) Mutations in the *O*-mannosyltransferase gene *POMT1* give rise to the severe neuronal migration disorder Walker-Warburg syndrome. *Am. J. Hum. Genet.* **71,** 1033–1043
27. van Reeuwijk, J., Janssen, M., van den Elzen, C., Beltran-Valero de Bernabé, D., Sabatelli, P., Merlini, L., Boon, M., Scheffer, H., Brockington, M., Muntoni, F., Huynen, M. A., Verrips, A., Walsh, C. A., Barth, P. G., Brunner, H. G., and van Bokhoven, H. (2005) POMT2 mutations cause α-dystroglycan hypoglycosylation and Walker-Warburg syndrome. *J. Med. Genet.* **42,** 907–912
28. Yoshida, A., Kobayashi, K., Manya, H., Taniguchi, K., Kano, H., Mizuno, M., Inazu, T., Mitsuhashi, H., Takahashi, S., Takeuchi, M., Herrmann, R., Straub, V., Talim, B., Voit, T., Topaloglu, H., Toda, T., and Endo, T. (2001) Muscular dystrophy and neuronal migration disorder caused by mutations in a glycosyltransferase, POMGnT1. *Dev. Cell* **1,** 717–724
29. Kobayashi, K., Nakahori, Y., Miyake, M., Matsumura K., Kondo-Iida, E., Nomura, Y., Segawa, M., Yoshioka, M., Saito, K., Osawa, M., Hamano, K., Sakakihara, Y., Nonaka, I., Nakagome, Y., Kanazawa, I., Nakamura, Y., Tokunaga, K., and Toda, T. (1998) An ancient retrotransposal insertion causes Fukuyama-type congenital muscular dystrophy. *Nature* **394,** 388–392
30. Brockington, M., Blake, D. J., Prandini, P., Brown, S. C., Torelli, S., Benson, M. A., Ponting, C. P., Estournet, B., Romero, N. B., Mercuri, E., Voit, T., Sewry, C. A., Guicheney, P., and Muntoni, F. (2001) Mutations in the fukutin-related protein gene (FKRP) cause a form of congenital muscular dystrophy with secondary laminin α2 deficiency and abnormal glycosylation of α-dystroglycan. *Am. J. Hum. Genet.* **69,** 1198–1209
31. Longman, C., Brockington, M., Torelli, S., Jimenez-Mallebrera, C., Kennedy, C., Khalil, N., Feng, L., Saran, R. K., Voit, T., Merlini, L., Sewry, C. A., Brown, S. C., and Muntoni, F. (2003) Mutations in the human LARGE gene cause MDC1D, a novel form of congenital muscular dystrophy with severe mental retardation and abnormal glycosylation of α-dystroglycan. *Hum. Mol. Genet.* **12,** 2853–2861
32. Bao, X., Kobayashi, M., Hatakeyama, S., Angata, K., Gullberg, D., Nakayama, J., Fukuda, M. N., and Fukuda, M. (2009) Tumor suppressor function of laminin-binding α-dystroglycan requires a distinct β3-*N*-acetylglucosaminyltransferase. *Proc. Natl. Acad. Sci. U.S.A.* **106,** 12109–12114
33. de Bernabé, D. B., Inamori, K., Yoshida-Moriguchi, T., Weydert, C. J., Harper, H. A., Willer, T., Henry, M. D., and Campbell, K. P. (2009) Loss of α-dystroglycan laminin binding in epithelium-derived cancers is caused by silencing of LARGE. *J. Biol. Chem.* **284,** 11279–11284
34. Nakagawa, N., Izumikawa, T., Kitagawa, H., and Oka, S. (2011) Sulfation of glucuronic acid in the linkage tetrasaccharide by HNK-1 sulfotransferase is an inhibitory signal for the expression of a chondroitin sulfate chain on thrombomodulin. *Biochem. Biophys. Res. Commun.* **415,** 109–113
35. Kanagawa, M., Nishimoto, A., Chiyonobu, T., Takeda, S., Miyagoe-Suzuki, Y., Wang, F., Fujikake, N., Taniguchi, M., Lu, Z., Tachikawa, M., Nagai, Y., Tashiro, F., Miyazaki, J., Tajima, Y., Takeda, S., Endo, T., Kobayashi, K., Campbell, K. P., and Toda, T. (2009) Residual laminin binding activity and enhanced dystroglycan glycosylation by LARGE in novel model mice to dystroglycanopathy. *Hum. Mol. Genet.* **18,** 621–631
36. Spanjaard, R. A., Ikeda, M., Lee, P. J., Charpentier, B., Chin, W. W., and Eberlein, T. J. (1997) Specific activation of retinoic acid receptors (RARs) and retinoid X receptors reveals a unique role for RARγ in induction of differentiation and apoptosis of S91 melanoma cells. *J. Biol. Chem.* **272,** 18990–18999
37. Barresi, R., Michele, D. E., Kanagawa, M., Harper, H. A., Dovico, S. A., Satz, J. S., Moore, S. A., Zhang, W., Schachter, H., Dumanski, J. P., Cohn, R. D., Nishino, I., and Campbell, K. P. (2004) LARGE can functionally bypass α-dystroglycan glycosylation defects in distinct congenital muscular dystrophies. *Nat. Med.* **10,** 696–703
38. Patnaik, S. K., and Stanley, P. (2005) Mouse large can modify complex *N*- and mucin *O*-glycans on α-dystroglycan to induce laminin binding. *J. Biol. Chem.* **280,** 20851–20859
39. Yamauchi, S., Mita, S., Matsubara, T., Fukuta, M., Habuchi, H., Kimata, K., and Habuchi, O. (2000) Molecular cloning and expression of chondroitin 4-sulfotransferase. *J. Biol. Chem.* **275,** 8975–8981
40. Okuda, T., Mita, S., Yamauchi, S., Fukuta, M., Nakano, H., Sawada, T., and Habuchi, O. (2000) Molecular cloning and characterization of GalNAc 4-sulfotransferase expressed in human pituitary gland. *J. Biol. Chem.* **275,** 40605–40613
41. Kanagawa, M., Saito, F., Kunz, S., Yoshida-Moriguchi, T., Barresi, R., Kobayashi, Y. M., Muschler, J., Dumanski, J. P., Michele, D. E., Oldstone, M. B., and Campbell, K. P. (2004) Molecular recognition by LARGE is essential for expression of functional dystroglycan. *Cell* **117,** 953–964
42. Brockington, M., Torelli, S., Prandini, P., Boito, C., Dolatshad, N. F., Longman, C., Brown, S. C., and Muntoni, F. (2005) Localization and functional analysis of the LARGE family of glycosyltransferases. Significance for muscular dystrophy. *Hum. Mol. Genet.* **14,** 657–665
43. Ong, E., Yeh, J. C., Ding, Y., Hindsgaul, O., Pedersen, L. C., Negishi, M., and Fukuda, M. (1999) Structure and function of HNK-1 sulfotransferase. Identification of donor and acceptor binding sites by site-directed mutagenesis. *J. Biol. Chem.* **274,** 25608–25612
44. Girard, J. P., Baekkevold, E. S., and Amalric, F. (1998) Sulfation in high endothelial venules. Cloning and expression of the human PAPS synthetase. *FASEB J.* **12,** 603–612
45. Mooy, C. M., Luyten, G. P., de Jong, P. T., Jensen, O. A., Luider, T. M., van der Ham, F., and Bosman, F. T. (1995) Neural cell adhesion molecule distribution in primary and metastatic uveal melanoma. *Hum. Pathol.* **26,** 1185–1190
46. Thies, A., Schachner, M., Berger, J., Moll, I., Schulze, H. J., Brunner, G., and Schumacher, U. (2004) The developmentally regulated neural crest-associated glycotope HNK-1 predicts metastasis in cutaneous malignant melanoma. *J. Pathol.* **203,** 933–939
47. Casado, J. G., Delgado, E., Patsavoudi, E., Durán, E., Sanchez-Correa, B., Morgado, S., Solana, R., and Tarazona, R. (2008) Functional implications of HNK-1 expression on invasive behavior of melanoma cells. *Tumour Biol.* **29,** 304–310
48. Stalnaker, S. H., Hashmi, S., Lim, J. M., Aoki, K., Porterfield, M., Gutierrez-Sanchez, G., Wheeler, J., Ervasti, J. M., Bergmann, C., Tiemeyer, M., and Wells, L. (2010) Site mapping and characterization of *O*-glycan structures on α-dystroglycan isolated from rabbit skeletal muscle. *J. Biol. Chem.* **285,** 24882–24891
49. Nilsson, J., Nilsson, J., Larson, G., and Grahn, A. (2010) Characterization of site-specific *O*-glycan structures within the mucin-like domain of α-dystroglycan from human skeletal muscle. *Glycobiology* **20,** 1160–1169
50. Stalnaker, S. H., Aoki, K., Lim, J. M., Porterfield, M., Liu, M., Satz, J. S., Buskirk, S., Xiong, Y., Zhang, P., Campbell, K. P., Hu, H., Live, D., Tiemeyer, M., and Wells, L. (2011) Glycomic analyses of mouse models of congenital muscular dystrophy. *J. Biol. Chem.* **286,** 21180–21190
51. Chiba, A., Matsumura, K., Yamada, H., Inazu, T., Shimizu, T., Kusunoki, S., Kanazawa, I., Kobata, A., and Endo, T. (1997) Structures of sialylated *O*-linked oligosaccharides of bovine peripheral nerve α-dystroglycan. The role of a novel *O*-mannosyl-type oligosaccharide in the binding of α-dystroglycan with laminin. *J. Biol. Chem.* **272,** 2156–2162
52. Yoshida-Moriguchi, T., Yu, L., Stalnaker, S. H., Davis, S., Kunz, S., Madson, M., Oldstone, M. B., Schachter, H., Wells, L., and Campbell, K. P. (2010) *O*-Mannosyl phosphorylation of α-dystroglycan is required for laminin binding. *Science* **327,** 88–92
53. Inamori, K., Yoshida-Moriguchi, T., Hara, Y., Anderson, M. E., Yu, L., and Campbell, K. P. (2012) Dystroglycan function requires xylosyl- and glucuronyltransferase activities of LARGE. *Science* **335,** 93–96

Biochemical and Biophysical Research Communications 424 (2012) 354–357

Contents lists available at SciVerse ScienceDirect

Biochemical and Biophysical Research Communications

journal homepage: www.elsevier.com/locate/ybbrc

Detection of the dystroglycanopathy protein, fukutin, using a new panel of site-specific monoclonal antibodies

Tracy A. Lynch [a,1,2], Le Thanh Lam [a,2], Nguyen thi Man [a,2], Kazuhiro Kobayashi [c,2], Tatsushi Toda [c], Glenn E. Morris [a,b,*]

[a] Wolfson Centre for Inherited Neuromuscular Disease, RJAH Orthopaedic Hospital, Oswestry, SY10 7AG, UK
[b] Institute for Science and Technology in Medicine, Keele University, UK
[c] Division of Neurology/Molecular Brain Science, Kobe University Graduate School of Medicine, Kobe 650-0017, Japan

ARTICLE INFO

Article history:
Received 25 June 2012
Available online 6 July 2012

Keywords:
Fukutin
Fukuyama muscular dystrophy
Monoclonal antibody
Dystroglycan
Dystroglycanopathy
Golgi
Phage-displayed peptide library
Epitope mapping

ABSTRACT

Mutations in the gene encoding fukutin protein cause Fukuyama muscular dystrophy, a severe congenital disorder that occurs mainly in Japan. A major consequence of the mutation is reduced glycosylation of alpha-dystroglycan, which is also a feature of other forms of congenital and limb-girdle muscular dystrophy. Immunodetection of endogenous fukutin in cells and tissues has been difficult and this has hampered progress in understanding fukutin function and disease pathogenesis. Using a new panel of monoclonal antibodies which bind to different defined sites on the fukutin molecule, we now show that fukutin has the predicted size for a protein without extensive glycosylation and is present at the Golgi apparatus at very low levels. These antibodies should enable more rapid future progress in understanding the molecular function of fukutin.

1. Introduction

Fukuyama-type congenital muscular dystrophy (FCMD: MIM 253800), one of the most prevalent autosomal recessive disorders in the Japanese population, was originally described clinically as a muscular dystrophy combined with cortical dysgenesis (micropolygyria) and ocular abnormalities [1]. The gene responsible for FCMD was identified on chromosome 9q31 by linkage analysis and positional cloning and was named fukutin [2,3]. A 3-kb retrotransposal insertion in the 3' non-coding region of the fukutin gene is the most common mutation in Japan, but other fukutin mutations occur outside Japan and cause various phenotypes, including Walker–Warburg syndrome (WWS: MIM 236670) and limb-girdle muscular dystrophy (LGMD) [4–6]. It is clear, therefore, that partial or complete loss of fukutin function can give rise to a wide spectrum of phenotypes with different severities.

Mutations in fukutin cause abnormal glycosylation of cell surface α-dystroglycan which in turn reduces its laminin-binding activity [7], but a direct catalytic function for fukutin has not been established. Transfected fukutin is targeted to the Golgi apparatus, where glycosylation events usually occur, by an amino-terminal transmembrane domain. Fukutin also binds directly to the enzyme POMGnT1 (*O*-mannose-β-1,2-*N*-acetylglucosaminyltransferase1) and the transmembrane domain is required for this interaction [8]. This suggests that fukutin mutations may affect αDG glycosylation by their influence on POMGnT1 [8], mutations in which are responsible for a related dystroglycanopathy, muscle-eye-brain disease (MEB: MIM 253280) [9]. Both POMGnT1 and the POMT1/2 complex have glycosyltransferase activities directly involved in synthesis of *O*-mannosyl sugar chains on α-DG [9,10]. Yoshida-Moriguchi and colleagues [11] reported that a phosphodiester-linked moiety on *O*-mannose of α-DG is defective in fukutin-deficient and other dystroglycanopathies and that this specific modification is necessary for laminin binding activity. The enzyme that carries out this modification has not been identified. An indirect role for fukutin in α-DG glycosylation remains a possibility. Thus, Tachikawa et al. [12] found that four pathogenic missense mutants of fukutin caused mis-localization to the endoplasmic reticulum (ER) instead of the Golgi, rather than having a direct effect on α-DG glycosylation. These mutants were able to localize correctly when mis-folding was inhibited. Zebrafish studies [13] have suggested that fukutin may also have a role in maintaining the Unfolded Protein Response (UPR) and this may contribute to the unique clinical features of Fukuyama MD.

* Corresponding author at: Wolfson Centre for Inherited Neuromuscular Disease, RJAH Orthopaedic Hospital, Oswestry, SY10 7AG, UK. Fax: +44 1691 404170.
E-mail address: glenn.morris@rjah.nhs.uk (G.E. Morris).
[1] Present address: Diagnostic Innovations Ltd., St. Asaph Business Park, St. Asaph, UK.
[2] These authors contributed equally to this work.

0006-291X/$ - see front matter © 2012 Elsevier Inc. All rights reserved.
http://dx.doi.org/10.1016/j.bbrc.2012.06.147

2. Materials and methods

A fukutin cDNA fragment (bases 60–1,494) containing the open reading frame was subcloned by PCR into the vector pEGFP-N1 (Clontech) and into pET vectors for bacterial expression [3]. Subfragments were cloned into pGEX vectors for bacterial expression as GST-fusion proteins. Monoclonal antibody production [14] and epitope mapping with phage-displayed peptide libraries [15] were performed as previously described. HeLa cells were grown as monolayers on tissue culture plastic Petri dishes or glass coverslips in DMEM with 10% fetal bovine serum. Immunoprecipitation and western blotting were performed as previously described [16]. Secondary antibodies were from DAKOpatts, Copenhagen.

3. Results

Balb/c mice were immunized either with full-length recombinant human fukutin or with a mixture of 4 GST-fusion proteins containing fukutin fragments (amino-acids 26–58, 177–220, 233–268 and 415–461). Sera from 3 out of 8 mice recognized a 54 kDa band on western blots of human muscle (Fig. 1). This is the predicted size for the unmodified amino-acid sequence of fukutin. However, experience with rabbit and goat antisera against fukutin (our unpublished data) showed that protein bands of this size on western blots are not always authentic fukutin. To select mice for hybridoma fusions, we therefore used an additional criterion: recognition of over-expressed GFP-fukutin at the Golgi apparatus (Fig. 2) to show that their sera contained anti-fukutin antibodies.

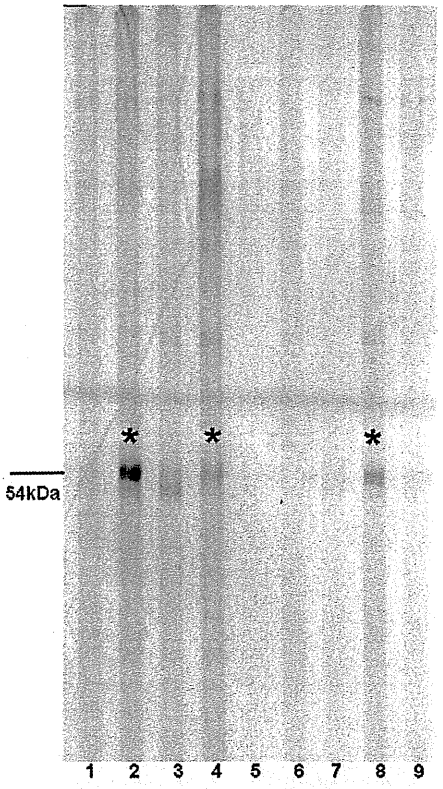

Fig. 1. Three mouse antisera recognize a 54 kDa protein in human muscle. An extract of normal human muscle was subjected to SDS–PAGE on a 3–12.5% gradient gel as a strip and antisera (0.07 ml of 1/100 in PBS) were applied in the lanes of a miniblotter. The position of a 54 kD marker is indicated and the three positive antisera are marked with an astérix. The lanes are as follows: (lanes 1–4), four mice immunized with mixture of GST-fukutin fragments, mice *"GST1 to 4"*; (lane 5) PBS control, (lane 6) normal mouse serum control, (lanes 7–9) three mice immunized with full-length fukutin, mice *"pETF1 to 3"*. *GST2* and *pETF2* were used for hybridoma fusions (see Table 1).

Four hybridoma fusions were performed using spleens from three mice (*pETF2, G70 and J41*) that responded to full-length protein and one mouse (*GST2*) that responded to the fragment mixture. Twelve mAbs that recognized recombinant fukutin in both ELISA and western blot are shown in Table 1; all except one were from the immunizations with full-length protein. None of the mAbs recognized endogenous 54 kDa fukutin on western blots. Seven of them did, however, recognize over-expressed GFP-fukutin at the Golgi apparatus (Table 1).

Because it seemed likely that endogenous fukutin was present at too low concentration in muscle for detection, we concentrated fukutin from HeLa cells by immunoprecipitation with a goat polyclonal antibody [16] and tested 14 mAbs by western blotting of this highly-enriched extract. Eleven of them reacted well with a single 54 kDa protein band, while three reacted only very weakly or not at all (Fig. 3). All mAbs were used at a concentration of about 1 μg/ml and immuno-precipitations using pre-immune serum as negative control showed that only the 54 kDa band is fukutin-specific (Fig. 3).

Epitope mapping of the binding sites on fukutin for the mAb panel was performed using phage-displayed random 15-mer peptide libraries [15]. In this method, only the amino-acids within the 15-mer peptide which are important for mAb binding match with the target sequence. Reactivity with phage-displayed peptides revealed six mapping groups, plus MANFU5 which would not react with any phage colonies (possibly a conformational epitope). Groups 1 (amino-acids 223–231: MANFU4), 2 (amino-acids 452–461: MANFU11 and 12) and 3 (amino-acids 182–187: MANFU7-10 inclusive) were mapped with confidence by matching 3 or 4 different peptides from the random library to the fukutin sequence (Fig. 4). Group 4 (MANFU2 and 3) reacted with a single peptide only, but with four sequential amino-acids matched (PHSR: amino-acids 243–246), this was unlikely to have occurred by chance. It was possible to place other mAbs into Groups 1, 5 or 6 by their reactivity with different phage peptides, even though it was not possible to match the phage peptides with the fukutin sequence in these cases, possibly because the epitope is conformation-dependent.

4. Discussion

The results are consistent with the view that fukutin is a very low abundance protein, required for glycosylation of α-dystroglycan at the Golgi, though not substantially-glycosylated itself. It

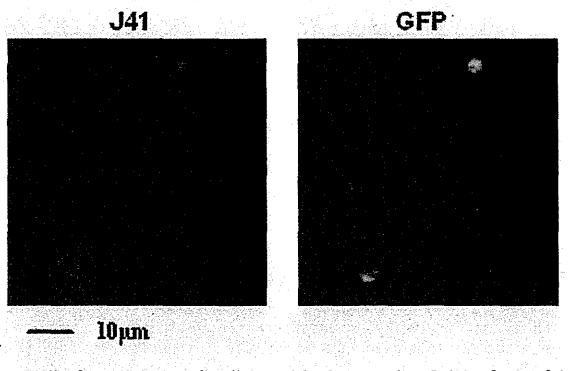

Fig. 2. Antibody staining co-localizes with GFP at the Golgi of GFP-fukutin-transfected HeLa cells. A HeLa cell-line expressing GFP-fukutin was grown on coverslips. After fixing with acetone-methanol, the cells were incubated with mouse antibody against fukutin (mouse number J41) followed by TRITC anti-(mouse Ig).

Table 1
Twelve monoclonal antibodies against fukutin. Column 1: Antibody name and clone number; column 2: intensity of western blot staining in Fig. 3; Column 3: name given to the mouse used for hybridoma production, *GST2* (mix) was immunized with the mixture of four fukutin fragments and the other three mice (*pETF2*, *G70* and *J41*) with full-length fukutin; Column 4: phage mapping: the epitope group allocated and amino-acid sequence of the epitope from Fig. 4; Column 5: HeLa-GFP IMF: reactivity at the Golgi in the *IMF* (immunofluorescence microscopy) experiment shown in Fig. 2, rated as either "*good*" (similar to Fig. 2) or "*poor*".

Antibody	Western Blot	Origin (name of mouse)	Phage mapping	HeLa-GFP IMF
MANFU1 7A2	++	GST2 (mix)	Group 6, clone	Poor
MANFU2 10F9	++	PETF2	Group 4 mapped AA243–246	Poor
MANFU3 4E6	+++	PETF2	Group 4 mapped AA243–246	Good
MANFU4 3C7	++	PETF2	Group 1, clone	Good
MANFU5 7H2	++	PETF2	No clones	Good
MANFU6 4H8	(w+)	PETF2	Group 5, clone	Poor
MANFU7 1B5	++	G70	Group 3 mapped AA180–187	Poor
MANFU8 2F5	++	G70	Group 3 mapped AA180–187	Good
MANFU9 4E12	++	G70	Group 3 mapped AA180–187	Good
MANFU10 5H10	++	G70	Group 3 mapped AA180–187	Poor
MANFU11 3E4	++	J41	Group 2 mapped AA452–461	Good
MANFU12 6B5	+++	J41	Group 2 mapped AA452–461	Good

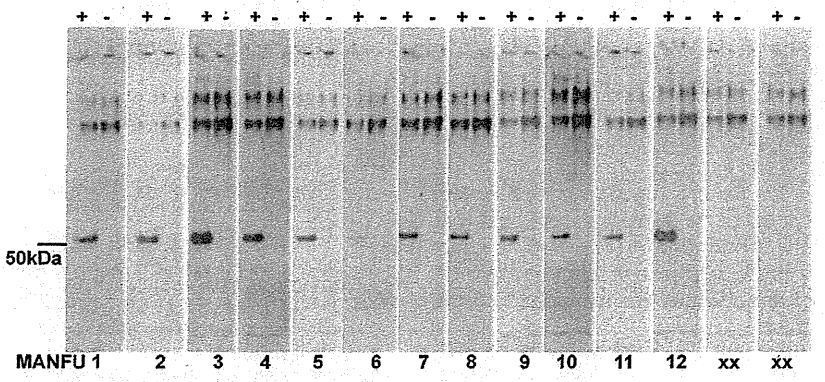

Fig. 3. Twelve mAbs recognize endogenous fukutin from HeLa cells after enrichment by immunoprecitation. HeLa cell extracts were immunoprecipitated with either a goat anti-fukutin serum (+) or with pre-immune control serum (−) and these were loaded in pairs for SDS–PAGE and western blotting with 14 different hybridoma culture supernatants adjusted to 1 μg/ml mouse Ig concn. Each lane of the gel contained all the protein immunoprecipitated from two 100 mm culture dishes of HeLa monolayers. The supernatants were MANFU1 to 12 (see Table 1) plus two negative hybridoma supernatants from the same fusions (XX). The fukutin band runs at the expected size, just above the 50 kDa Mr. marker.

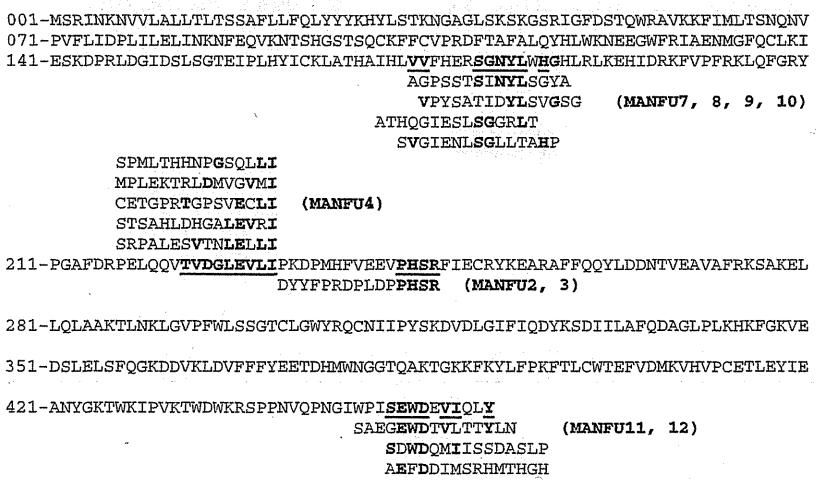

Fig. 4. Epitope mapping of eight mAbs to specific binding sites on fukutin. The mAbs were attached to Petri dishes coated with anti-(mouse Ig) and used to select phage displaying random 15-mer peptides on their surface [15]. After determining the mAb specificity of each selected phage clone, the DNA was sequenced to determine the amino-acid sequence of the peptide displayed. The complete 461aa sequence of fukutin is shown, together with the 15-mer phage peptide sequences that matched it. In each case, the peptides were recognized specifically by the named mAbs only and not by other mAbs in the panel. Where several peptides are shown alongside several mAbs (e.g. MANFU7-10), ALL the mAbs recognized ALL the peptides.

may have an enzymatic function, but the alternative possibility that it has an essential supporting role in dystroglycan glycosylation by modifying the localization or activity of other proteins has not been ruled out.

Detection of endogenous fukutin by mAbs required pre-enrichment of cell extracts (Fig 3), but the 54 kD band was confidently identifiable as authentic fukutin because it was recognized by mAbs against five different fukutin epitopes. Only monoclonal antibodies against different epitopes on fukutin make it possible to distinguish with confidence between endogenous fukutin and a more abundant cross-reacting protein on western blots, as we have shown for another low-abundance antigen, DMPK [17]. Although polyclonal mouse antisera were able to detect a 54 kD protein on western blots of total cell extracts (Fig. 1), we are unable to prove that this is authentic fukutin.

The localization of over-expressed fukutin very specifically to the Golgi (Fig. 2) and its detection at this site by mAbs against five different fukutin epitopes (Table 1) suggests that low endogenous protein levels can explain the failure of mAbs to detect fukutin in untransfected cells. The alternative possibility that epitope masking at the Golgi prevents antibody access to endogenous fukutin appears less likely when mAbs against five different fukutin epitopes give the same result.

We have shown that at least six or seven different epitopes are recognized by the panel of 12 mAbs (Table 1) and four regions of the fukutin amino-acid sequence have been shown to contain binding sites for 9 mAbs using phage-displayed peptide libraries (Fig. 4). The two mAbs against the extreme C-terminus of fukutin may be especially valuable for further functional studies. The remaining three mAbs may recognize conformational epitopes that either select no clones from the peptide library (MANFU5) or select clones that do not match the linear sequence of fukutin (MANFU1 and 6). Table 1 shows that epitope diversity was increased by using spleens from four different mice.

The mAbs described in this study are freely available for academic research from the MDA Monoclonal Antibody Resource (www.glennmorris.org/mabs.htm).

Acknowledgments

Monoclonal antibody production was supported by a Grant from the Muscular Dystrophy Campaign UK (GEM) and epitope mapping was supported by a grant from the Muscular Dystrophy Association USA (GEM).

References

[1] Y. Fukuyama, M. Osawa, M., H. Suzuki, Congenital progressive muscular dystrophy of the Fukuyama type – clinical, genetic and pathological considerations, Brain Dev. 3 (1981) 1–29.
[2] T. Toda, M. Segawa, Y. Nomura, I. Nonaka, et al., Localization of a gene for Fukuyama type congenital muscular dystrophy to chromosome 9q31-33, Nat. Genet. 5 (1993) 283–286.
[3] K. Kobayashi, Y. Nakahori, M. Miyake, K. Matsumura, et al., An ancient retrotransposal insertion causes Fukuyama-type congenital muscular dystrophy, Nature 394 (1998) 388–392.
[4] D. Beltrán-Valero de Bernabé, H. van Bokhoven, E. van Beusekom, W. van den Akker, et al., J. Med. Genet. 40 (2003) 845–848.
[5] C. Godfrey, D. Escolar, M. Brockington, E.M. Clement, et al., Fukutin gene mutations in steroid-responsive limb girdle muscular dystrophy, Ann. Neurol. 60 (2006) 603–610.
[6] C. Godfrey, E. Clement, R. Mein, M. Brockington, et al., Refining genotype phenotype correlations in muscular dystrophies with defective glycosylation of dystroglycan, Brain 130 (2007) 2725–2735.
[7] D.E. Michele, R. Barresi, M. Kanagawa, F. Saito, et al., Post-translational disruption of dystroglycan-ligand interactions in congenital muscular dystrophies, Nature 418 (2002) 417–422.
[8] H. Xiong, K. Kobayashi, M. Tachikawa, H. Manya, et al., Molecular interaction between fukutin and POMGnT1 in the glycosylation pathway of alpha-dystroglycan, Biochem. Biophys. Res. Commun. 350 (2006) 935–941.
[9] A. Yoshida, K. Kobayashi, H. Manya, K. Taniguchi, et al., Muscular dystrophy and neuronal migration disorder caused by mutations in a glycosyltransferase, POMGnT1, Dev. Cell 1 (2001) 717–724.
[10] H. Manya, A. Chiba, A. Yoshida, X. Wang, et al., Demonstration of mammalian protein O-mannosyltransferase activity: coexpression of POMT1 and POMT2 required for enzymatic activity, Proc. Natl. Acad. Sci. U. S. A. 101 (2004) 500–505.
[11] T. Yoshida-Moriguchi, L. Yu, S.H. Stalnaker, S. Davis, et al., O-mannosyl phosphorylation of alpha-dystroglycan is required for laminin binding, Science 327 (2010) 88–92.
[12] M. Tachikawa, M. Kanagawa, C.C. Yu, K. Kobayashi, T. Toda, Mislocalization of Fukutin protein by disease-causing missense mutations can be rescued with treatments directed at folding amelioration, J. Biol. Chem. 287 (2012) 8398–8406.
[13] Y.Y. Lin, R.J. White, S. Torelli, S. Cirak, F. Muntoni, D.L. Stemple, Zebrafish Fukutin family proteins link the unfolded protein response with dystroglycanopathies, Hum. Mol. Genet. 20 (2011) 1763–1775.
[14] Thi Man Nguyen, G.E. Morris, A rapid method for generating large numbers of high-affinity monoclonal antibodies from a single mouse, in: J.M. Walker (Ed.), The Protein Protocols Handbook, third ed., Humana Press, Totowa, NJ, 2009, pp. 1961–1974.
[15] A. Pereboev, G.E. Morris, Reiterative screening of phage display peptide libraries for epitope mapping, in: G.E. Morris (Ed.), Epitope Mapping Protocols, Meth. Mol. Biol., vol. 66, Humana Press, Totowa, NJ, 1996, pp. 195–206.
[16] M. Taniguchi-Ikeda, K. Kobayashi, M. Kanagawa M, et al., Pathogenic exon-trapping by SVA retrotransposon and rescue in Fukuyama muscular dystrophy, Nature 478 (2011) 127–131.
[17] Le Thanh Lam, Y.C.N. Pham, Thi Man Nguyen, G.E. Morris, Characterization of a monoclonal antibody panel shows that the myotonic dystrophy protein kinase, DMPK, is expressed almost exclusively in muscle and heart, Hum. Mol. Genet. 9 (2000) 2167–2173.

Journal of Human Genetics (2012) 57, 515–522

www.nature.com/jhg

ORIGINAL ARTICLE

Screening of genes involved in chromosome segregation during meiosis I: *in vitro* gene transfer to mouse fetal oocytes

Makiko Tsutsumi[1], Hiroe Kowa-Sugiyama[1], Hasbaira Bolor[1], Hiroshi Kogo[1], Hidehito Inagaki[1], Tamae Ohye[1], Kouji Yamada[1], Mariko Taniguchi-Ikeda[2], Tatsushi Toda[2] and Hiroki Kurahashi[1]

The events that take place during the prophase of meiosis I are essential for the correct segregation of homologous chromosomes. Defects in these processes likely contribute to infertility or recurrent pregnancy loss in humans. To screen for candidate genes for reproductive failure due to meiotic defects, we have analyzed the gene expression patterns in fetal, neonatal and adult gonads of both male and female mice by microarray and thereby identified 241 genes that are expressed specifically during prophase of meiosis I. Combined with our previous data obtained from developing spermatocytes, a total of 99 genes were identified that are upregulated in early prophase I. We confirmed the meiotic prophase I-specific expression of these genes using qRT-PCR. To further screen this panel for candidate genes that fulfill important roles in homologous pairing, synapsis and recombination, we established a gene transfer system for prophase I oocytes in combination with *in vitro* organ culture of ovaries, and successfully determined the localization of the selected genes. This gene set can thus serve as a resource for targeted sequence analysis via next-generation sequencing to identify the genes associated with human reproduction failure due to meiotic defects.
Journal of Human Genetics (2012) **57**, 515–522; doi:10.1038/jhg.2012.61; published online 31 May 2012

Keywords: infertility; meiosis; microarray

INTRODUCTION

Infertility is a serious clinical condition for couples who desire to have children. It is estimated that ~15% of couples attempting conception suffer from some form of infertility, and that in ~30% of these cases there is no definitive cause.[1] Although some infertile couples are successfully treated with assisted reproductive technology, some couples can go through years of infertility treatment without success. Another serious problem in reproduction is recurrent pregnancy loss (RPL), which affects ~5% of couples.[2] The cause of RPL cannot be determined in up to 50% of the cases.[3,4] As multiple factors underlie the etiology of infertility and RPL, these disorders are believed to be polygenic, whereas single-gene abnormalities have been demonstrated to be a cause of reproductive defects in animal models.[5] The heterogeneous and complex characteristics of RPL have made the causes challenging to elucidate. Moreover, it is difficult to identify the responsible gene(s) using pedigree analysis because the genetic factors that cause a susceptibility to infertility will be poorly transmitted through the germline.

Mutations or polymorphisms in genes associated with meiosis are potentially good candidates as genetic causes of infertility because they would create no other defects other than reproductive defects. Approaches involving the sequencing of candidate genes have enabled the identification of a few meiotic genes that are causal for infertility or RPL.[6–9] Further analyses of these candidate genes will be necessary to better understand the genetic basis of human infertility and RPL. It is likely also that many other genes involved in meiosis in mammals, and that that remain to be identified, have a role in these disorders.

Unlike mitotic division, homologous chromosomes segregate from each other during meiosis I. The formation of DNA double-strand breaks, subsequent repair by homologous recombination and maintenance of the resultant chiasma between homologous chromosomes until anaphase are essential for correct segregation. Studies in mouse models have revealed that impairment of these processes during early meiosis results in apoptosis or aneuploidy.[10] The extensive apoptosis of gametes leads to infertility, whereas aneuploidy in gametes, whether the abnormality is derived from a homologous or sister chromosome segregation error, contributes to RPL or to the birth of offspring with congenital defects. Interestingly, males and females differ in terms of meiotic defect outcomes. In males, infertility due to extensive apoptosis is the most predominant outcome, whereas segregation

[1]Division of Molecular Genetics, Institute for Comprehensive Medical Science, Fujita Health University, Aichi, Japan and [2]Division of Neurology/Molecular Brain Science, Kobe University Graduate School of Medicine, Hyogo, Japan
Correspondence: Dr H Kurahashi, Division of Molecular Genetics, Institute for Comprehensive Medical Science, Fujita Health University, 1-98 Dengakugakubo, Kutsukake-cho, Toyoake, Aichi 470-1192, Japan.
E-mail: kura@fujita-hu.ac.jp
Received 8 March 2012; revised 24 April 2012; accepted 2 May 2012; published online 31 May 2012

errors in maternal chromosomes often results in aneuploid oocytes.[11] It has been reasonably hypothesized that this sexual dimorphism might be due to a prolonged meiotic prophase I in females or due to differences in checkpoint robustness.[12,13] However, despite its importance to understanding the differences in the molecular mechanisms underlying correct segregation between males and females, there is little currently known about oogenesis because of the limited availability of oocytes.

To further investigate the etiology of infertility and RPL in humans, and the mechanisms of chromosome segregation in mammals, we have previously performed expression profiling analysis of mouse spermatocytes.[14] We focused on screening for genes upregulated in the transition to leptotene/zygotene spermatocytes from spermatogonia to identify the factors controlling the correct segregation of chromosomes during meiosis I. We thereby identified a total of 726 genes, MLZ (male leptotene and zygotene)-001-726. However, this MLZ gene panel actually included many spermatogenesis-specific genes, which hindered further analyses. In our current study, the gene expression profiles of both male and female gonads undergoing meiosis I were examined by microarray analysis to exclude the effects of male-specific genes in the MLZ gene set. This enabled an enrichment of meiotic genes and prevented the exclusion of female factors.

MATERIALS AND METHODS

Microarray analysis

All animal experiments were approved by the Animal Care and Use Committee at Fujita Health University. Total RNA was extracted from male and female gonads of C57BL6 mice at 15.5 days postcoitum (dpc), neonatal day 1 and 10 weeks postpartum. Microarray experiments were performed as described previously,[14] except that the GeneChip Mouse Genome 430 2.0 array (Affymetrix, Santa Clara, CA, USA) was used in this study. Microarray data analyses were performed using Microsoft Excel (Microsoft, Redmond, WA, USA), Genespring software, version 11 (Silicon Genetics, Redwood City, CA, USA) and Affymetrix Microarray Suite, Version 5 (MAS5, Affymetrix). All data were subjected to per chip and per gene normalization, and then used for further analysis. Annotations of all filtered transcripts were updated using Affymetrix NetAffx (http://www.netaffx.com), based on the July 2011 annotation update. Microarray data were deposited in the GEO database according to the MIAME Guidelines and assigned the accession number GSE35734.

Real-time RT-PCR

First-strand cDNAs were synthesized as described previously.[14] Real-time RT-PCR assays were also performed as described previously.[15] The primer sets used in these experiments are listed in Supplementary Table 1.

Expression of epitope-tagged proteins

The entire coding region of each selected candidate gene was obtained by RT-PCR and individually cloned into the pFLAG-CMV2 vector (Sigma-Aldrich, St Louis, MO, USA). Plasmids were dissolved in electroporation buffer (125 mM NaCl, 5 mM KCl, 1.5 mM $MgCl_2$, 10 mM glucose and 20 mM Hepes, pH 7.4)[16] at a concentration of 3.5 $\mu g\,\mu l^{-1}$. Mouse ovaries with attached mesonephroses at 13.5 dpc were removed. After injection of the tissues with plasmids suspended in L-15 medium, the ovaries were electroporated as described previously[17] with some modifications. Briefly, after injection, ovaries with mesonephroses were placed between electrodes (CUY501G2, Nepa Gene, Chiba, Japan) with a small volume of electroporation buffer. A 45-V, 50-ms rectangular pulse was charged 5 times at 100-ms intervals using an electroporator (CUY21SC, Nepa Gene). The tissues were then cultured for 2 days as described previously[17] except that Transwell membrane inserts (polycarbonate membrane, 24-mm diameter, 3.0-μm pore size, Corning, Corning, NY, USA) and minimum essential medium-alpha medium (Invitrogen, Carlsbad, CA, USA) containing 10% fetal bovine serum, and supplemented with penicillin and streptomycin were used. For expression in mouse spermatocytes, the plasmids were introduced into the testis by *in vivo* electroporation as described previously,[9] and these tissues were dissected out for immunostaining 2 days later.

Immunofluorescence microscopy

Testis frozen sections were fixed in acetone for 15 min and then washed three times in phosphate-buffered saline (PBS). After blocking with 10% normal donkey serum in PBS for 30 min at room temperature, primary antibodies were applied as described below. Squashed oocytes were prepared as described previously.[18,19] Slides were incubated with blocking buffer (5% normal donkey serum and 5% normal goat serum in PBS), and then incubated with primary antibodies diluted in PBS at 4 °C overnight at the following dilutions: rabbit anti-FLAG (D-8, Santa Cruz Biotechnology, Santa Cruz, CA, USA), 1:1000; guinea-pig anti-SYCP3 antiserum,[15] 1:5000. The slides were then washed three times in PBS for 15 min, and incubated with the following secondary antibodies to enable detection by fluorescence microscopy: Alexa 594-conjugated donkey anti-rabbit IgG and Alexa 488-conjugated goat anti-guinea-pig IgG (Invitrogen), or aminomethylcoumarin acetate-conjugated donkey anti-guinea-pig IgG (Jackson ImmunoReasearch, West Grove, PA, USA). The secondary antibodies were diluted in PBS and incubated at room temperature for 30 min. After again washing three times in PBS, slides were mounted in Mowiol/DABCO (Sigma-Aldrich) with or without DAPI (4′-6-diamidino-2-phenylindole) (0.5 $\mu g\,ml^{-1}$) and observed under a fluorescence microscope (Axio Imager M1, Carl Zeiss, Jena, Germany). Images were processed using Adobe Photoshop software (Adobe Systems, San Jose, CA, USA).

RESULTS

Enrichment of a candidate gene set for meiosis I prophase in mouse gonads

The gene expression profiles of gonads from a 15.5-dpc fetal male (FM), 15.5-dpc fetal female (FF), neonatal day 1 male (NM), neonatal day 1 female (NF), 10-week-old male (AM) and 10-week-old female (AF) mice were examined by microarray analysis. To screen for meiotic prophase I-related genes, we performed filtering as described in Figure 1a. First, we eliminated male-specific genes using flag calls as follows. Genes with a 'present' or 'marginal' call in either FF or NF were selected, which would be expected to include genes expressed in female meiosis I but no male-specific genes. Likewise genes with a 'present' or 'marginal' call in AM were selected to eliminate female-specific genes. These genes were further filtered by comparing the expression levels in AM with those in FM, NM and AF, followed by filtering of genes for which the expression levels in FF were more than threefold higher than those of AF. Thus, we extracted a total of 267 genes that were upregulated in both male and female gonads undergoing meiotic prophase I. After correcting for redundancy, 241 non-redundant genes were identified and these are listed in Supplementary Table 2. Within this panel, there were 99 matches for genes in the MLZ gene set (Figure 1b), and these are listed in Supplementary Table 3.

The composition of the final 99 selected genes is summarized in Table 1. Among these gene candidates, 76 are named and the remaining 23 are previously uncharacterized. Among the named genes, 17 genes (~22%) have been reported to show meiosis-preferred expression, with only six genes known to display testis-preferred expression. On the other hand, among the 578 named genes in the MLZ gene set identified previously, 101 genes have been demonstrated to show testis-preferred expression.[14] This indicates that the male-specific genes had mostly been excluded from the MLZ gene set in this study. Significantly, most of the genes known to function in meiotic prophase I were included in our final 99 gene panel, as shown in Table 2. These data suggest that the MLZ gene set had been successfully enriched with genes involved in the prophase of meiosis I. However, three genes, *Mei1*, *Msh5* and *Rec8*, in spite of their

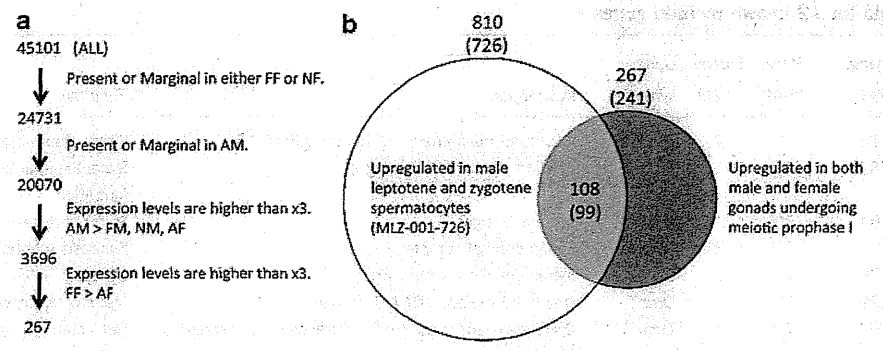

Figure 1 Generation of a gene set that is upregulated during meiotic prophase I. (a) Strategy for filtering genes that are upregulated in the mouse gonads undergoing meiotic prophase I. 'Present' and 'Marginal' are detection calls of the MAS5 algorithm, which is an indicator of expression. The numbers of genes selected by each step are indicated. (b) Venn diagram indicating the number of selected genes using two criteria: the MLZ gene set identified previously by Kogo *et al.*[14] (left) and genes identified in the current analysis (right).

Table 1 Classification of 99 (241)[a] candidate meiotic genes from the mouse

Genes	*Characteristics*	*Number*	*Subtotal*	*Total*
Known	Meiosis-preferred expression	17 (20)		
	Testis-preferred expression	6 (6)		
	Others	53 (157)	76 (183)	
Unknown	Others	23 (58)	23 (58)	99 (241)

[a]Numbers in the parentheses are that of the 241 gene set.

well-known functional association with chromosomal behavior in meiosis, did not appear among these 99 genes, but were included in the initial screen of 241 genes. We thus performed subsequent analyses also on this larger 241 gene set.

Developmental gene expression profiling of the female mouse gonads

To explore which of the candidate genes in our data sets show a similar expression profile with known meiotic genes, we grouped the 241 and 99 gene panels discretely into 4 clusters using k-means clustering analysis. Three groups of microarray data from mouse female gonads were applied to this analysis in order to focus on the expression level changes between the early (15.5 dpc) and late (neonatal day 1) stages of prophase I. The results of our clustering of the 241 genes are shown in Figure 2a and Supplementary Table 2. For the genes in cluster A, the expression levels are higher in NF than in FF or AF. Fifty genes were grouped in cluster A, but none with known functions in meiotic chromosomal behavior and only 11 that overlapped with the 99 selected meiotic genes. Hence, cluster A appeared to contain female-predominant genes expressed in the later stages of oogenesis. Cluster B contained as many as 110 genes, but only five with meiosis-specific expression, suggesting that many of the genes in this cluster may not be specifically associated with meiotic chromosomal behavior. The gene expression patterns for cluster C were found to be similar to those of cluster B, although the expression levels in FF were higher than the genes in cluster B. Cluster C contains 10 meiotic genes including *Spo11*, *Rec8* and *Sycp3*. Genes in cluster D exhibited the highest expression levels in FF compared with the other clusters. Among the 27 genes in this cluster, 22 overlapped with the 99 gene panel, and five of these genes are well-known meiotic genes including *Dmc1* and *Smc1b*. These results confirm the enrichment of genes involved in meiosis I prophase in the 99 gene set.

Similar clustering was also performed for the 99 selected genes (Figure 2b and Supplementary Table 3). The expression levels of the genes assigned to cluster 1 were high in FF but decreased in NF. *Spo11*, *Dmc1* and *Atm*, which are the key enzymes involved in the formation and repair of meiotic DNA double-strand breaks, were included in this cluster. The expression levels of the genes in cluster 2 were higher in both FF and NF than those of the cluster 1 genes. This cluster includes a cohesin component, *Smc1b*. Hence, clusters 1 and 2 may include genes involved in early stages of prophase during meiosis I. Cluster 3 contains genes whose expression did not switch off until neonatal day 1. *Sycp1*, *Sycp3* and *Syce1* are included in this cluster, which indicates that the genes in cluster 3 are necessary through to the later stages of prophase I. The genes in cluster 4 showed lower expression in both FF and NF than the genes of any other clusters. *Syce2* is the only gene in this cluster to have been functionally established as a meiotic gene, indicating that our 99 gene panel still included non-meiotic genes that were categorized into cluster 4.

Real-time RT-PCR analysis of selected genes

We randomly selected nine genes from the 99 gene panel with no known function in meiosis (Table 3). These genes were analyzed by real-time RT-PCR to verify whether they were meiosis-specific (Figure 3). We used RNA extracts from the gonads of FM, FF, AM and AF mice, because we were focusing only on the early stages of prophase I. The expression of *Sycp3*, a meiosis-specific gene, showed high levels in FF and AM, but low levels in FM, AF and somatic tissues (Figure 3a). MLZ-175, MLZ-611, MLZ-638 and MLZ-675 showed meiotic expression patterns that were similar to *Sycp3* (Figure 3a). MLZ-254, MLZ-326 and MLZ-344 showed testis-predominant expression patterns (Figure 3b). MLZ-352 and MLZ-617 showed testis-predominant expression patterns, but were found to be expressed also in the adult mouse ovary (Figure 3b). In 11 of the known meiotic genes listed in Supplementary Table 3, the expression ratios of FF to AF derived from the microarray analysis were high (>22-fold). These genes ranked in the top 25 among the 99 gene panel in terms of the ratios of FF to AF. Among the nine genes we analyzed by real-time RT-PCR, MLZ-611 and MLZ-675 ranked also in the top 25, and both showed meiotic expression patterns (Figure 3a). These results suggest that genes with a higher expression ratio of FF to AF among our 99 selected genes are strong candidates as functional genes in meiotic chromosomal behavior.

Table 2 Microarray data for 12 known meiotic genes

Probe set ID	Fold change (FF/AF)	Rank in 99	Cluster in 99	Gene symbol	Description	Function	Expression
1449253_at	329.15	1	2	*Smc1b*	Structural maintenance of chromosomes 1B	Sister chromatid cohesion	Meiotic
1450292_a_at	130.82	6	1	*Hormad1*	HORMA domain containing 1	Synaptonemal complex formation	Meiotic
1460229_at	68.84	10	1	*Stag3*	Stromal antigen 3	Sister chromatid cohesion	Meiotic
1427291_at	52.27	12	3	*Sycp1*	Synaptonemal complex protein 1	Synapsis (central element)	Meiotic
1449534_at	35.78	14	3	*Sycp3*	Synaptonemal complex protein 3	Synapsis (lateral element)	Meiotic
1420335_at	27.29	19	1	*Dmc1*	Disrupted meiotic cDNA 1 homolog	Meiotic recombination	Meiotic
1453872_at	27.03	20	1	*Dmrtc2*	Doublesex- and mab-3-related transcription factor-like family C2	Sex chromatin transformation in male	Meiotic
1419511_at	23.93	24	1	*Msh4*	mutS homolog 4	Meiotic recombination	Meiotic
1417021_a_at	11.17	37	1	*Spo11*	Sporulation protein 11	Meiotic recombination	Meiotic
1429270_a_at	5.14	67	4	*Syce2*	Synaptonemal complex central element protein 2	Synapsis (central element)	Meiotic
1427197_at	4.12	74	1	*Atr*	Ataxia telangiectasia and Rad3 related	Meiotic recombination	Ubiquitous
1449170_at	3.03	99	3	*Piwil2*	piwi-like homolog 2	Gene regulation	Meiotic

Abbreviations: AF, 10-week-old female; FF, 15.5-dpc fetal female.

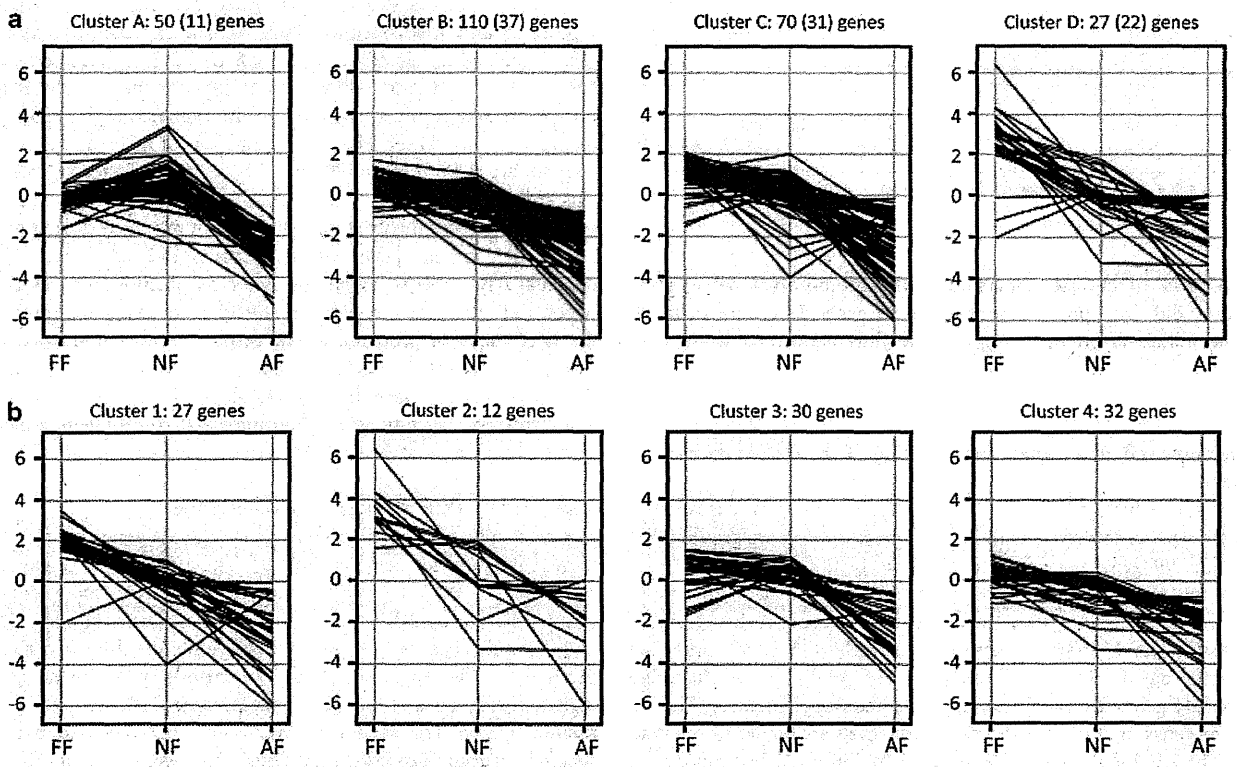

Figure 2 K-means clustering for the gene expression profiles of the 241 and 99 gene panels derived from the developmental mouse ovary. (**a**) Clustering of the 241 gene panel. Numbers indicate the gene numbers of the 241 panel, whereas those in parentheses denote the candidates in the 99 gene panel. (**b**) Clustering of the 99 gene panel. Numbers indicate the gene numbers of this panel. Normalized signal intensities are shown on the y axis. Because some genes have more than one probe set on the microarray platform, the sum of the four clusters exceeds 241 or 99 (see Supplementary Tables 2 and 3).

Subcellular localization of the epitope-tagged proteins expressed in mouse oocytes

To perform a further screen for meiotic genes that might be involved in chromosome segregation, we examined the subcellular localization of the protein products encoded by our candidate genes using vectors expressing epitope-tagged proteins. In our previous study, HEK293 cells had been used as a heterologous transfection system.[14] However, ectopically expressed SYCP3 generates a loop-like structure not only in the nucleus but also in the cytoplasm in somatic cell lines, which had not correctly reflected its intrinsic localization pattern in a previous report.[9] Therefore, in our current analyses we introduced a plasmid DNA expressing FLAG-tagged SYCP3 into adult mouse testis by *in vivo* electroporation. The FLAG-tagged SYCP3 protein product was detectable in the nuclei of pachytene spermatocytes by

Table 3 Validation results for nine of the candidate genes in this study

Name	Probe set ID	Fold change (FF/AF)	Rank in 99	Representative public ID	Gene symbol	Gene title	RT-PCR	Subcellular localization
MLZ-175	1423576_a_at	8.31	48	AV283456	*Fhl4*	Four and a half LIM domains 4	Meiotic	ND
MLZ-254	1429366_at	8.4	47	AK005720	*Lrrc34*	Leucine rich repeat containing 34	Testis	ND
MLZ-326	1426806_at	3.8	79	AV313559	*Obfc2a*	Oligonucleotide/oligosaccharide-binding fold containing 2A	Testis	ND
MLZ-344	1432386_a_at	6.85	55	AK005673	*Phf7*	PHD finger protein 7	Testis	ND
MLZ-352	1429936_at	5.94	62	BC019481	*Pih1d2*	PIH1 domain containing 2	Testis	ND
MLZ-611	1432458_at	196.87	3	AK005864	*1700011F14Rik*	RIKEN cDNA 1700011F14 gene	Meiotic	Nuclear and cytoplasm
MLZ-617	1436593_at	9.75	44	AV260052	*1700016K19Rik*	RIKEN cDNA 1700016K19 gene	Testis	ND
MLZ-638	1453942_at	11.58	35	AK007250	*1700123I01Rik*	RIKEN cDNA 1700123I01 gene	Meiotic	Cytoplasm
MLZ-675	1431648_at	58.82	11	AK015924	*4930528F23Rik*	RIKEN cDNA 4930528F23 gene	Meiotic	ND

Abbreviations: AF, 10-week-old female; FF, 15.5-dpc fetal female; ND, not determined.

immunofluorescence with anti-FLAG antibodies, and the staining pattern was found to be similar to that of endogenous SYCP3, reflecting that it is a component of the synaptonemal complex (Figure 4a). As we were focusing on the genes associated with female meiosis in the analysis, the same plasmid was introduced into a fetal mouse ovary by electroporation followed by *in vitro* organ culture. Overexpressed SYCP3 with a FLAG-tag was found to localize in the nuclei of leptotene oocytes as also demonstrated in spermatocytes (Figure 4b). These results indicate that epitope-tagged proteins that are overexpressed in both spermatocytes and oocytes show a pattern that reflects their intrinsic subcellular localization during meiosis. We thus applied this method to oocytes to examine the subcellular localization of unknown genes.

Plasmids expressing FLAG-tagged protein products for two candidate genes (MLZ-611 and MLZ-638) were introduced into oocytes (Figure 4b). The amino acid sequences encoded by these genes had no obvious nuclear localization signals and no distinct motifs other than coiled-coils. The protein encoded by MLZ-638 was observed in the cytoplasm of the oocytes. The localization of the MLZ-611 protein showed two patterns: both nuclear and cytoplasmic staining, and cytoplasmic only. The nuclear localization of MLZ-611 suggests a possible role in chromosome segregation.

DISCUSSION

To date, studies of global gene expression profiles of isolated oocytes have been mostly limited to metaphase II oocytes or earlier oocytes at the primordial follicle stage.[20–23] Although gene expression profile data for fetal or neonatal ovaries have been provided in mouse and human, and have enabled the analysis of genes involved in the initiation of meiosis, the sex differentiation of the gonad, early meiosis, and ovarian and follicle development, investigations of meiotic prophase I have been lacking.[24–28] In yeast, it is estimated that ~150 genes may be meiosis-specific.[29,30] In our current study, we screened 99 genes that are upregulated during prophase in meiosis I. Despite the fact that this gene number is less than one-seventh of the previous MLZ gene set, most of the well-known genes associated with meiotic chromosome behavior, sister chromatid cohesion, synapsis and homologous recombination, are included in this select gene panel. This indicates that our select 99 gene panel includes many other unknown meiotic genes, the functional elucidation of which will likely facilitate an increased understanding of the mechanisms underlying the sexual dimorphism between males and females. For further screening, 76 uncharacterized genes among these 99 genes is a reasonable number for individual validation by qRT-PCR. In addition, genes showing high FF to AF expression ratios by microarray should have priority in this respect.

Expression profiling using k-means clustering revealed that well-established meiotic genes were grouped into the same clusters, depending on their functions. Our clustering analysis of the initial 241 candidate gene panel showed that most of the known meiotic genes in this set grouped into two clusters, C and D. Hence, genes in these clusters that did not overlap with the 99 gene series may include genes that are upregulated after the zygotene stage and therefore warrant further analysis. Cluster 2, exhibiting the highest expression level in FF and NF among the four clusters established for the smaller 99 gene panel, included only one functionally known meiotic gene, *Smc1b*. This gene is important for maintaining the chiasma until adulthood, although its expression is clearly detectable only during the fetal stages and is barely evident in later stages in the female.[31] As the loading of SMC1B onto chromosomes begins at the leptotene stage during prophase I to establish meiotic cohesion, this protein needs to remain functional during a long meiotic arrest period in which it is not replenished.[19,32] The high expression of *Smc1b* transcripts in NF mice implies that robust cohesion might be established by this stage. A lack of turnover of the meiotic cohesin protein is considered to contribute to age-related chromosome segregation errors in oocytes.[32–34] The molecular mechanisms that maintain or disrupt meiotic cohesion have remained unclear for many decades. However, the candidate genes in cluster 2 in our current study may assist with our understanding of this complex phenomenon going forward.

Transient expression assays of epitope-tagged proteins to examine their subcellular localizations in oocytes would also likely assist with a determination of whether the molecules are engaged in chromosome behavior by direct observation of nuclear localization. The possible effect of the expression levels to the resultant subcellular localization might be overcome by observation of cells with various expression levels. As the efficiency of gene transfer for each gene varied from 2–3 cells to 20–30 cells per a litter, optimization of the condition for introduction might be necessary for each gene. To our knowledge, this is the first report to screen for genes of interest and then functionally characterize some of these candidates via their introduction into mouse oocytes during prophase I. Using this gene transfer system, the functions of uncharacterized gene can begin to be predicted if the localization of their encoded proteins is a unique nuclear domain, for

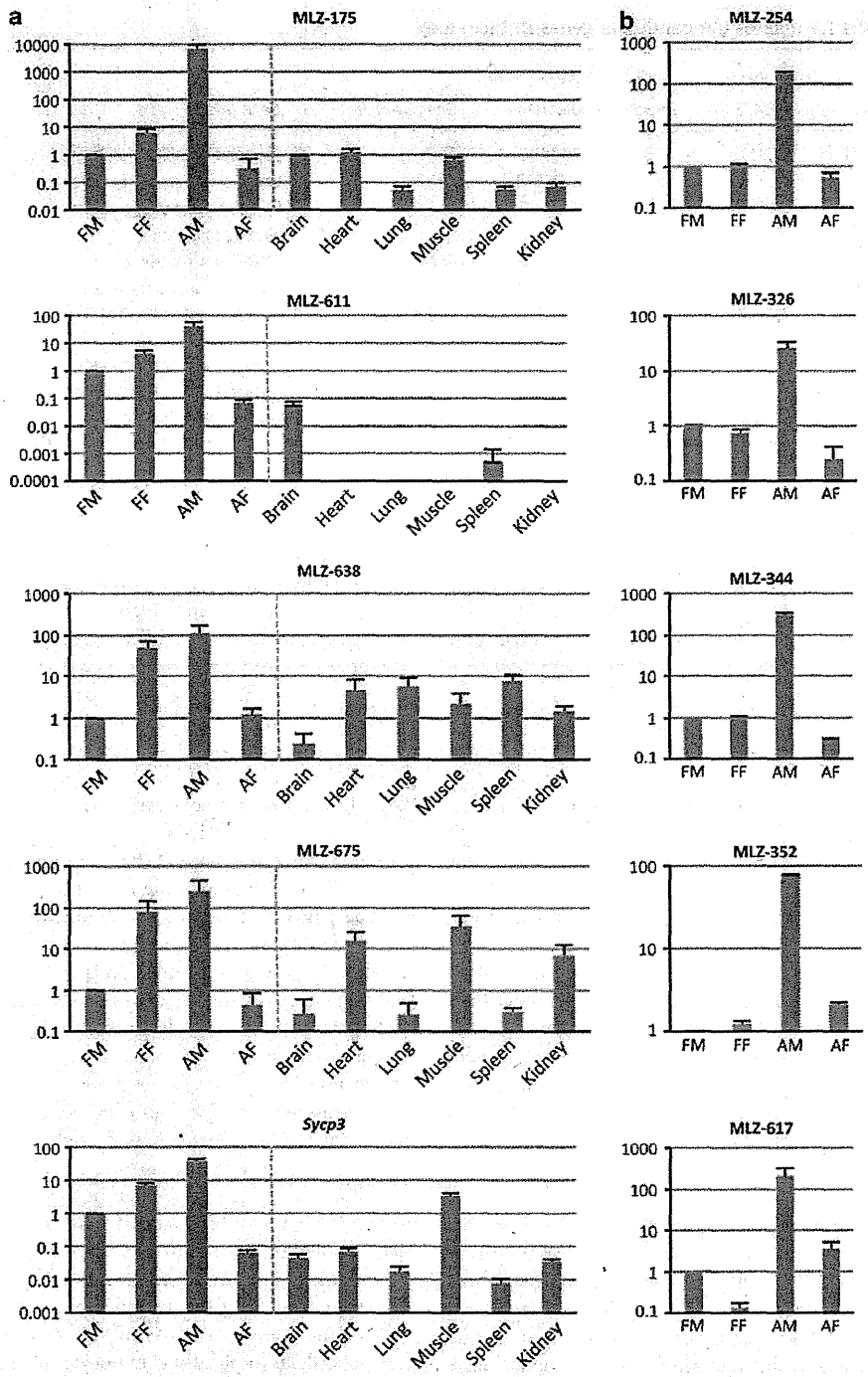

Figure 3 Real-time RT-PCR analysis of selected candidate genes using RNA from fetal gonads obtained from male and female mice at 15.5 dpc; adult gonads obtained from male and female mice at 10 weeks postpartum and somatic tissues. (**a**) Genes exhibiting meiotic expression patterns. (**b**) Genes exhibiting testis-predominant expression patterns. Expression ratios relative to the FM are shown on the y axis. Samples were run in triplicate, and error bars represent the standard deviation.

example, at the centromeres or chiasmata on meiotic chromosomes. Further, when a mutation has been identified in individuals with infertility or RPL, introduction of the mutant gene into oocytes in this way would readily enable functional analysis without the need to establish a knock-in mouse.

Also in our current analysis, we have identified that an uncharacterized gene, MLZ-611, may function in homologous chromosome segregation on the basis of its localization at the nucleus during prophase I. Recently, a bioinformatics approach using data from the published microarray analyses of gene expression during prophase I

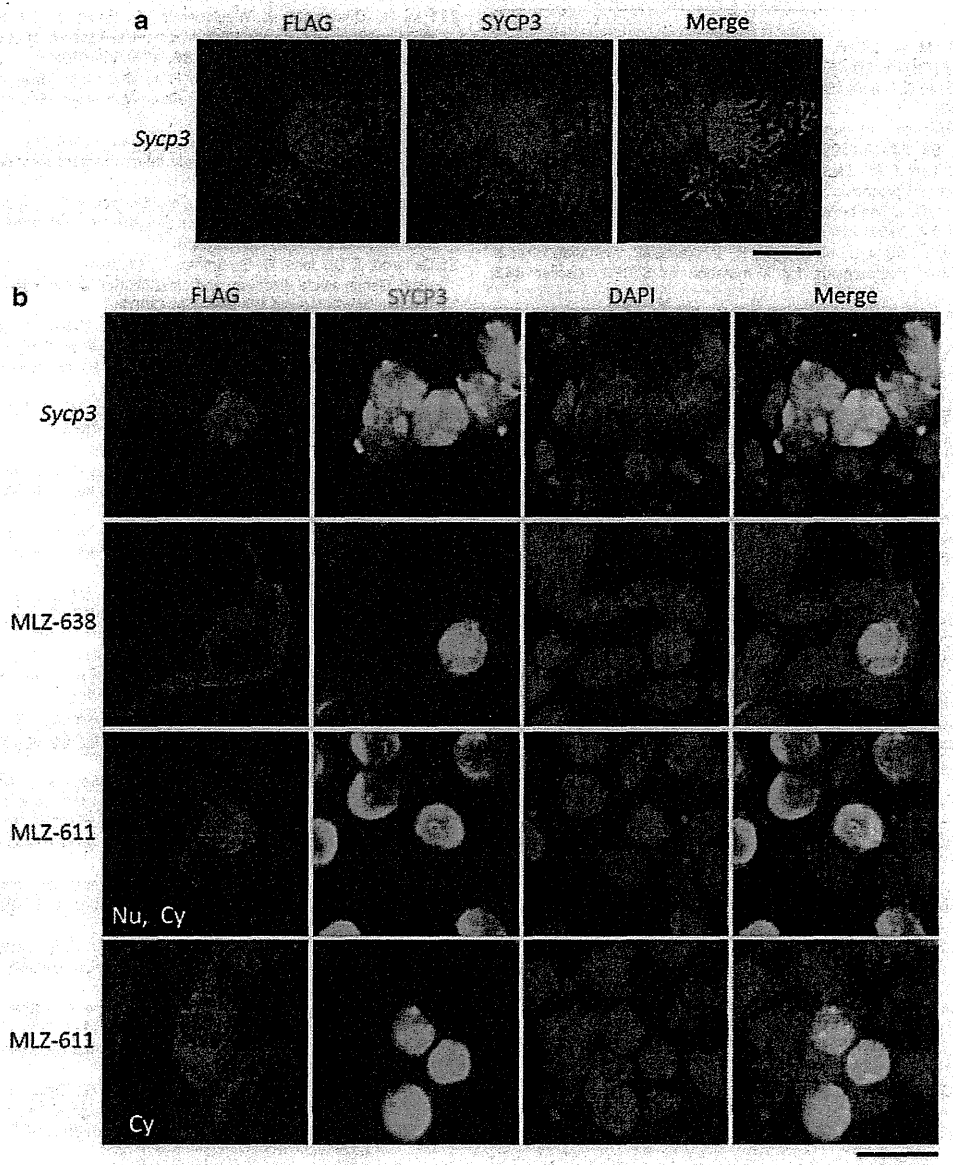

Figure 4 Subcellular localization of candidate meiotic gene protein products. Plasmids expressing FLAG-tagged proteins were introduced into mouse testis or ovarian tissues. (**a**) Immunostaining of testis frozen sections using anti-FLAG antibodies (red) and anti-SYCP3 antiserum (blue). Bar, 10 μm. (**b**) Squashed oocytes were analyzed by immunostaining with anti-FLAG antibodies (red), anti-SYCP3 antiserum (green), and nuclear counterstaining was performed with DAPI (blue). Nu, nucleus; Cy, cytoplasm. Bar, 20 μm.

has provided a cohort of candidate meiotic genes.[35] The authors of this report performed expression profiles of male and female gonads from mouse and human, and compared these patterns to detect conserved co-expression networks. Interestingly, MLZ-611 has a co-expression link with *Sycp3*, and MLZ-638 has co-expression links with *Smc1b*, *Sycp3*, *Hormad2*, and *Dmc1* across mouse and human systems. This indicates that MLZ-611 and MLZ-638 have potential functional connections with well-known meiotic genes in human.

Our final goal in the present study was to identify genes that may have a role in human infertility or RPL. Genes in our candidate lists that are verified as meiotic genes will be further assessed in the future using high-throughput mutational analysis involving targeted next-generation sequencing of genomic DNA from patients with reproductive problems. Recently, exome sequencing has been widely applied to the identification of causative mutations for human diseases.[36–38] However, this approach has been mainly limited to analyses of rare diseases because it is still too costly at present, to screen for mutations responsible for common diseases such as infertility or RPL in this way. Reducing the number of genes to be analyzed, as well as employing simultaneous analysis of multiple samples using barcoded primers assigned to each patient,[39] will allow the genome analyses to be conducted more cost-effectively and more rapidly.

ACKNOWLEDGEMENTS

We thank Dr Hiroki Kano and Ms Chiaki Shimizu for technical assistance. These studies were supported by a grant-in-aid for Scientific Research from the Ministry of Education, Culture, Sports, Science, and Technology of Japan, and a grant from the Hori Information Science Promotion Foundation.

1 Smith, S., Pfeifer, S. M. & Collins, J. A. Diagnosis and management of female infertility. *JAMA* **290,** 1767–1770 (2003).
2 Sierra, S. & Stephenson, M. Genetics of recurrent pregnancy loss. *Semin. Reprod. Med.* **24,** 17–24 (2006).
3 Stephenson, M. D. Frequency of factors associated with habitual abortion in 197 couples. *Fertil. Steril.* **66,** 24–29 (1996).
4 Li, T. C., Makris, M., Tomsu, M., Tuckerman, E. & Laird, S. Recurrent miscarriage: aetiology, management and prognosis. *Hum. Reprod. Update* **8,** 463–481 (2002).
5 Matzuk, M. M. & Lamb, D. J. The biology of infertility: research advances and clinical challenges. *Nat. Med.* **14,** 1197–1213 (2008).
6 Miyamoto, T., Hasuike, S., Yogev, L., Maduro, M. R., Ishikawa, M., Westphal, H. *et al.* Azoospermia in patients heterozygous for a mutation in SYCP3. *Lancet* **362,** 1714–1719 (2003).
7 Christensen, G. L., Ivanov, I. P., Atkins, J. F., Mielnik, A., Schlegel, P. N. & Carrell, D. T. Screening the SPO11 and EIF5A2 genes in a population of infertile men. *Fertil. Steril.* **84,** 758–760 (2005).
8 Mandon-Pépin, B., Touraine, P., Kuttenn, F., Derbois, C., Rouxel, A., Matsuda, F. *et al.* Genetic investigation of four meiotic genes in women with premature ovarian failure. *Eur. J. Endocrinol.* **158,** 107–115 (2008).
9 Bolor, H., Mori, T., Nishiyama, S., Ito, Y., Hosoba, E., Inagaki, H. *et al.* Mutations of the SYCP3 gene in women with recurrent pregnancy loss. *Am. J. Hum. Genet.* **84,** 14–20 (2009).
10 Cohen, P. E., Pollack, S. E. & Pollard, J. W. Genetic analysis of chromosome pairing, recombination, and cell cycle control during first meiotic prophase in mammals. *Endocr. Rev.* **27,** 398–426 (2006).
11 Hassold, T., Hall, H. & Hunt, P. The origin of human aneuploidy: where we have been, where we are going. *Hum. Mol. Genet.* **16,** R203–R208 (2007).
12 Kurahashi, H., Bolor, H., Kato, T., Kogo, H., Tsutsumi, M., Inagaki, H. *et al.* Recent advance in our understanding of the molecular nature of chromosomal abnormalities. *J. Hum. Genet.* **54,** 253–260 (2009).
13 Kogo, H., Tsutsumi, M., Ohye, T., Inagaki, H., Abe, T. & Kurahashi, H. HORMAD1-dependent checkpoint/surveillance mechanism eliminates asynaptic oocytes. *Genes Cells* **17,** 439–454 (2012).
14 Kogo, H., Kowa-Sugiyama, H., Yamada, K., Bolor, H., Tsutsumi, M., Ohye, T. *et al.* Screening of genes involved in chromosome segregation during meiosis I: toward the identification of genes responsible for infertility in humans. *J. Hum. Genet.* **55,** 293–299 (2010).
15 Tsutsumi, M., Kogo, H., Kowa-Sugiyama, H., Inagaki, H., Ohye, T. & Kurahashi, H. Characterization of a novel mouse gene encoding an SYCP3-like protein that relocalizes from the XY body to the nucleolus during prophase of male meiosis I. *Biol. Reprod* **85,** 165–171 (2011).
16 Kawabata, I., Umeda, T., Yamamoto, K. & Okabe, S. Electroporation-mediated gene transfer system applied to cultured CNS neurons. *Neuroreport* **15,** 971–975 (2004).
17 Nakamura, Y., Yamamoto, M. & Matsui, Y. Introduction and expression of foreign genes in cultured mouse embryonic gonads by electroporation. *Reprod. Fertil. Dev.* **14,** 259–265 (2002).
18 Page, J., Suja, J. A., Santos, J. L. & Rufas, J. S. Squash procedure for protein immunolocalization in meiotic cells. *Chromosome Res.* **6,** 639–642 (1998).
19 Prieto, I., Tease, C., Pezzi, N., Buesa, J. M., Ortega, S., Kremer, L. *et al.* Cohesin component dynamics during meiotic prophase I in mammalian oocytes. *Chromosome Res.* **12,** 197–213 (2004).
20 Hamatani, T., Falco, G., Carter, M. G., Akutsu, H., Stagg, C. A., Sharov, A. A. *et al.* Age-associated alteration of gene expression patterns in mouse oocytes. *Hum. Mol. Genet.* **13,** 2263–2278 (2004).
21 Pan, H., O'brien, M. J., Wigglesworth, K., Eppig, J. J. & Schultz, R. M. Transcript profiling during mouse oocyte development and the effect of gonadotropin priming and development *in vitro*. *Dev. Biol.* **286,** 493–506 (2005).
22 Kocabas, A. M., Crosby, J., Ross, P. J., Otu, H. H., Beyhan, Z., Can, H. *et al.* The transcriptome of human oocytes. *Proc. Natl Acad. Sci. USA* **103,** 14027–14032 (2006).
23 Grøndahl, M. L., Yding Andersen, C., Bogstad, J., Nielsen, F. C., Meinertz, H. & Borup, R. Gene expression profiles of single human mature oocytes in relation to age. *Hum. Reprod.* **25,** 957–968 (2010).
24 Small, C. L., Shima, J. E., Uzumcu, M., Skinner, M. K. & Griswold, M. D. Profiling gene expression during the differentiation and development of the murine embryonic gonad. *Biol. Reprod.* **72,** 492–501 (2005).
25 Gallardo, T. D., John, G. B., Shirley, L., Contreras, C. M., Akbay, E. A., Haynie, J. M. *et al.* Genomewide discovery and classification of candidate ovarian fertility genes in the mouse. *Genetics* **177,** 179–194 (2007).
26 Olesen, C., Nyeng, P., Kalisz, M., Jensen, T. H., Møller, M., Tommerup, N. *et al.* Global gene expression analysis in fetal mouse ovaries with and without meiosis and comparison of selected genes with meiosis in the testis. *Cell. Tissue. Res.* **328,** 207–221 (2007).
27 Houmard, B., Small, C., Yang, L., Naluai-Cecchini, T., Cheng, E., Hassold, T. *et al.* Global gene expression in the human fetal testis and ovary. *Biol. Reprod.* **81,** 438–443 (2009).
28 Hogarth, C. A., Mitchell, D., Evanoff, R., Small, C. & Griswold, M. Identification and expression of potential regulators of the mammalian mitotic-to-meiotic transition. *Biol. Reprod.* **84,** 34–42 (2011).
29 Chu, S., DeRisi, J., Eisen, M., Mulholland, J., Botstein, D., Brown, P. O. *et al.* The transcriptional program of sporulation in budding yeast. *Science* **282,** 699–705 (1998).
30 Primig, M., Williams, R. M., Winzeler, E. A., Tevzadze, G. G., Conway, A. R., Hwang, S. Y. *et al.* The core meiotic transcriptome in budding yeasts. *Nat. Genet.* **26,** 415–423 (2000).
31 Hodges, C. A., Revenkova, E., Jessberger, R., Hassold, T. J. & Hunt, P. A. SMC1beta-deficient female mice provide evidence that cohesins are a missing link in age-related nondisjunction. *Nat. Genet.* **37,** 1351–1355 (2005).
32 Revenkova, E., Herrmann, K., Adelfalk, C. & Jessberger, R. Oocyte cohesin expression restricted to predictyate stages provides full fertility and prevents aneuploidy. *Curr. Biol.* **20,** 1529–1533 (2010).
33 Tachibana-Konwalski, K., Godwin, J., van der Weyden, L., Champion, L., Kudo, N. R., Adams, D. J. *et al.* Rec8-containing cohesin maintains bivalents without turnover during the growing phase of mouse oocytes. *Genes Dev.* **24,** 2505–2516 (2010).
34 Chiang, T., Schultz, R. M. & Lampson, M. A. Meiotic origins of maternal age-related aneuploidy. *Biol. Reprod.* **86,** 1–7 (2012).
35 Su, Y., Li, Y. & Ye, P. Mammalian meiosis is more conserved by sex than by species: conserved co-expression networks of meiotic prophase. *Reproduction* **142,** 675–687 (2011).
36 Bamshad, M. J., Ng, S. B., Bigham, A. W., Tabor, H. K., Emond, M. J., Nickerson, D. A. *et al.* Exome sequencing as a tool for Mendelian disease gene discovery. *Nat. Rev. Genet.* **12,** 745–755 (2011).
37 Ku, C. S., Naidoo, N. & Pawitan, Y. Revisiting Mendelian disorders through exome sequencing. *Hum. Genet.* **129,** 351–370 (2011).
38 Singleton, A. B. Exome sequencing: a transformative technology. *Lancet Neurol.* **10,** 942–946 (2011).
39 Parameswaran, P., Jalili, R., Tao, L., Shokralla, S., Gharizadeh, B., Ronaghi, M. *et al.* A pyrosequencing-tailored nucleotide barcode design unveils opportunities for large-scale sample multiplexing. *Nucleic Acids Res.* **35,** e130 (2007).

Supplementary Information accompanies the paper on Journal of Human Genetics website (http://www.nature.com/jhg)

INTERNAL MEDICINE

□ CASE REPORT □

Anti-Hu-associated Paraneoplastic Encephalomyelitis with Esophageal Small Cell Carcinoma

Toshihiko Shirafuji[1], Fumio Kanda[1], Kenji Sekiguchi[1], Masatsugu Higuchi[1], Hiroshi Yokozaki[2], Keiko Tanaka[3], Hitoshi Takahashi[4] and Tatsushi Toda[1]

Abstract

A 63-year-old woman had anti-Hu-associated paraneoplastic encephalomyelitis (anti-Hu syndrome) caused by esophageal small cell carcinoma (SCC). The patient developed bilateral limbic encephalitis, followed by myelitis, brain stem encephalitis, and autonomic failure. Extensive examination demonstrated SCC of the abdominal lymph nodes that was retrospectively diagnosed as metastasis of esophageal SCC on autopsy. The neuropathological findings were characterized by widespread neuronal loss and gliosis in the central nervous system, as well as patchy loss of myelin and axons in the spinal nerve roots with perivascular lymphocytic infiltration. This is the first detailed clinical and neuropathological report of anti-Hu syndrome caused by esophageal SCC.

Key words: anti-Hu-associated paraneoplastic encephalomyelitis, esophageal small cell carcinoma, multiple lesions

(Intern Med 51: 2423-2427, 2012)
(DOI: 10.2169/internalmedicine.51.6884)

Introduction

Anti-Hu-associated paraneoplastic encephalomyelitis (anti-Hu syndrome) is the most frequent remote effect of cancer, potentially affecting the entire nervous system (1-3). Overall, 61-87% of anti-Hu syndrome cases were associated with pulmonary small cell carcinoma (SCC) (1-5). Only a few cases of anti-Hu syndrome associated with extra-pulmonary SCC have been reported. Anti-Hu syndrome related to SCC of the esophagus is extremely rare (2).

While a common clinical manifestation of the anti-Hu syndrome is sensory neuronopathy, 70% of patients have multiple clinical neurological symptoms and 34% of patients have 3 or more areas of involvement in the nervous system (3) during the course of the disease. There have been only a few reports which discuss multiple regional involvement in central and peripheral nervous systems (6, 7).

A case of anti-Hu syndrome with various paraneoplastic neurological syndromes, including, limbic encephalitis, subacute necrotizing myelitis, and brain stem encephalitis is presented. This is the first detailed clinical and neuropathological report of anti-Hu syndrome with esophageal SCC.

Case Report

A 63-year-old woman who complained of amnesia for one month was referred to our hospital for further examinations. On neurological examination, disorientation and emotional instability were evident. Cortical symptoms, such as aphasia or apraxia, were absent. The Mini-Mental State Examination (MMSE) score was 12/30. The total-intelligence quotient (IQ) was 73 (verbal IQ 79, performance IQ 68) on the Revised Wechsler Adult Intelligence Scale (WAIS-R).

Neurological examination revealed mild weakness of hip flexor bilaterally. Reflexes were increased in bilateral biceps and patellar tendons, and the right Achilles tendon, but were decreased in bilateral triceps and left Achilles tendons. Bilateral plantar responses were indifferent. There was no ataxia or sensory impairment.

[1]Division of Neurology, Kobe University Graduate School of Medicine, Japan, [2]Division of Surgical Pathology, Kobe University Graduate School of Medicine, Japan, [3]Department of Neurology, Kanazawa Medical University, Japan and [4]Department of Pathology, Brain Research Institute, University of Niigata, Japan
Received for publication November 5, 2011; Accepted for publication May 6, 2012
Correspondence to Dr. Toshihiko Shirafuji, tshirafuji@phoenix.kobe-u.ac.jp

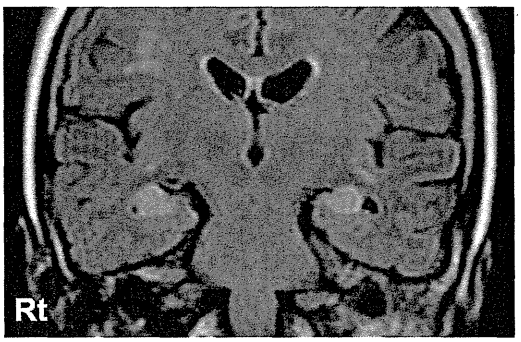

Figure 1. A FLAIR image of the brain MRI on admission shows high signal intensities in bilateral medial temporal lobes including the hippocampus, amygdala, and white matter.

Abdominal CT showed two, 2 to 3 cm diameter, round lymph nodes enhanced with gadolinium. A FLAIR image of the brain showed high signal intensities in the white matter and bilateral medial temporal lobes including the hippocampus and amygdala (Fig. 1). Laboratory tests revealed an increased concentration of serum pro-gastrin-releasing peptide (proGRP) at 69 pg/mL (<45 pg/mL), but serum neuron-specific enolase (NSE) was within normal limits. Cerebrospinal fluid contained 5 white blood cells/μL. Protein and IgG concentrations were 69 mg/dL and 9.4 mg/dL, respectively, and oligoclonal bands were positive in cerebrospinal fluid. Anti-Hu antibody was confirmed in the patient's serum at a titer >2,000. Anti-Yo, -Ri, -CV2, -Tr, -Ma2, and amphiphysin antibodies were negative. Anti-nucleus of the systemic organ antibody, anti-undetermined neuro-histology antibody, anti-ganglioside antibodies, and anti-voltage gated potassium channel antibody were also negative. The patient had HLA B51, one of the HLA B7 supertypes, consistent with a previous report (8).

To obtain a histological diagnosis, biopsy of the abdominal lymph node swelling was performed at 3 weeks. Microscopic examination of the biopsied abdominal lymph node revealed metastasis of SCC. After the biopsy, the patient needed mechanical ventilation due to respiratory muscle weakness. Since the serum proGRP returned to the normal range after the biopsy, chemotherapy was not started.

At week 3, muscular weakness of all extremities progressed, rendering her bedridden at week 5. Neurological examination revealed severe weakness of the upper extremities (grade 2) and the lower extremities (grade 1). Fasciculations were evident and deep tendon reflexes were decreased in all extremities. Bilateral plantar responses were indifferent. The sensory system was normal. Cerebrospinal fluid contained 3 white blood cells/μL. Protein and IgG concentrations were 186 mg/dL and 30.1 mg/dL, respectively, in the cerebrospinal fluid. Nerve conduction studies revealed reduction in amplitude of the compound muscle action potentials in the median nerves with normal motor nerve conduction velocities. The amplitudes of the sensory nerve action potentials and the sensory conduction velocities of the median and sural nerves were normal. Needle electromyography showed many fasciculation potentials with few fibrillation potentials and positive sharp waves (fib/PSW) before the biopsy. Many fib/PSW with a few fasciculation potentials in the right biceps brachii were observed during the progression of the muscular weakness. No waxing or waning phenomenon was observed with repetitive nerve stimulation.

Neither intravenous immunoglobulin infusion therapy (400 mg/kg daily for 5 days) at week 5 nor intravenous methyl-prednisolone pulse therapy (1,000 mg daily for 3 days) at week 10 showed any benefit for her condition.

At weeks 6 to 10, impairment of cranial nerves VI, VII, IX, and X developed and were followed by autonomic malfunctions including orthostatic hypotension, unstable pulse rate, and decreased bowel sounds. The patient developed a succession of bouts of pneumonia at weeks 21, 30, and 40. At week 21, her consciousness level deteriorated to a deep coma. There was flaccid paralysis of all extremities. All tendon reflexes were disappeared. Bilateral plantar responses were indifferent. There was no involuntary movement. The patient died of sepsis 10 months after the onset of the neurological symptoms.

Autopsy findings

A general autopsy was performed about 14 hours after death, at which time the brain weighed 1,280 g. The brain and spinal cord were fixed with 10% formalin, and multiple tissue blocks were embedded in paraffin. Histological examination was performed on 4-μm-thick sections using several stains, including hematoxylin and eosin, Klüver-Barrera, Bodian, and Holtzer. Immunohistochemical examination was also carried out: the spinal cord sections, with the anterior and posterior nerve roots, and esophageal cancer tissue sections were immunostained using an antibody against phosphorylated neurofilament (SMI-31, Sternberger Monoclonals, Bethesda, MD, USA).

Macroscopic findings

A general autopsy revealed a tumor arising in the middle part of the esophagus (Fig. 2) with metastasis to the regional para-aortic lymph nodes, which was later shown histopathologically to be SCC; the tumor cells were positive for cytokeratin, CD56 and synaptophysin (data not shown). There was no lymph node involvement other than the regional lymph nodes, consistent with the limited disease (LD).

The brain, including brain stem, cerebellum, and spinal cord, was almost entirely soft and pale. The cerebral cortex showed thinning and pale-brownish discoloration, being more marked in the lateral temporal lobe. The subcortical white matter also showed a coarse granular appearance.

Microscopic findings

Histopathological examination of the brain and spinal cord revealed apparent neuronal loss and gliosis in almost the entire cerebral cortex, brainstem lower motor neuron nuclei [severe in the oculomotor (III) and hypoglossal (XII)

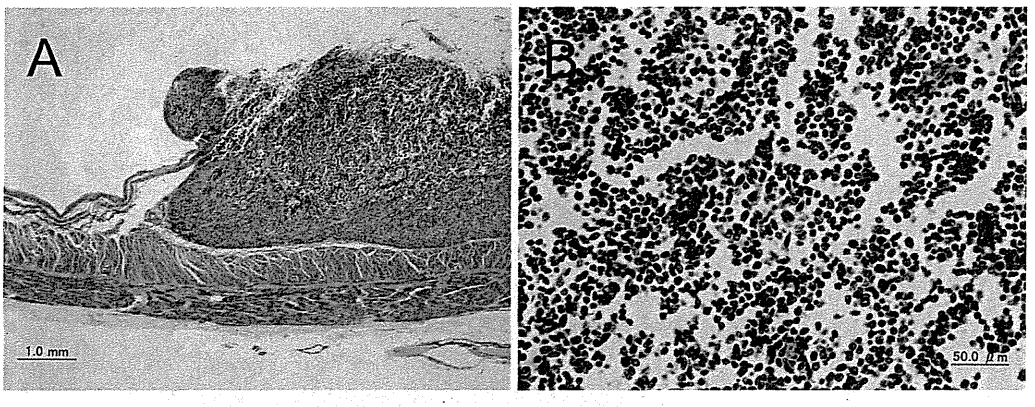

Figure 2. A tumor in the middle region of the esophagus (A), consisting of small cancer cells (B) (Hematoxylin and Eosin staining).

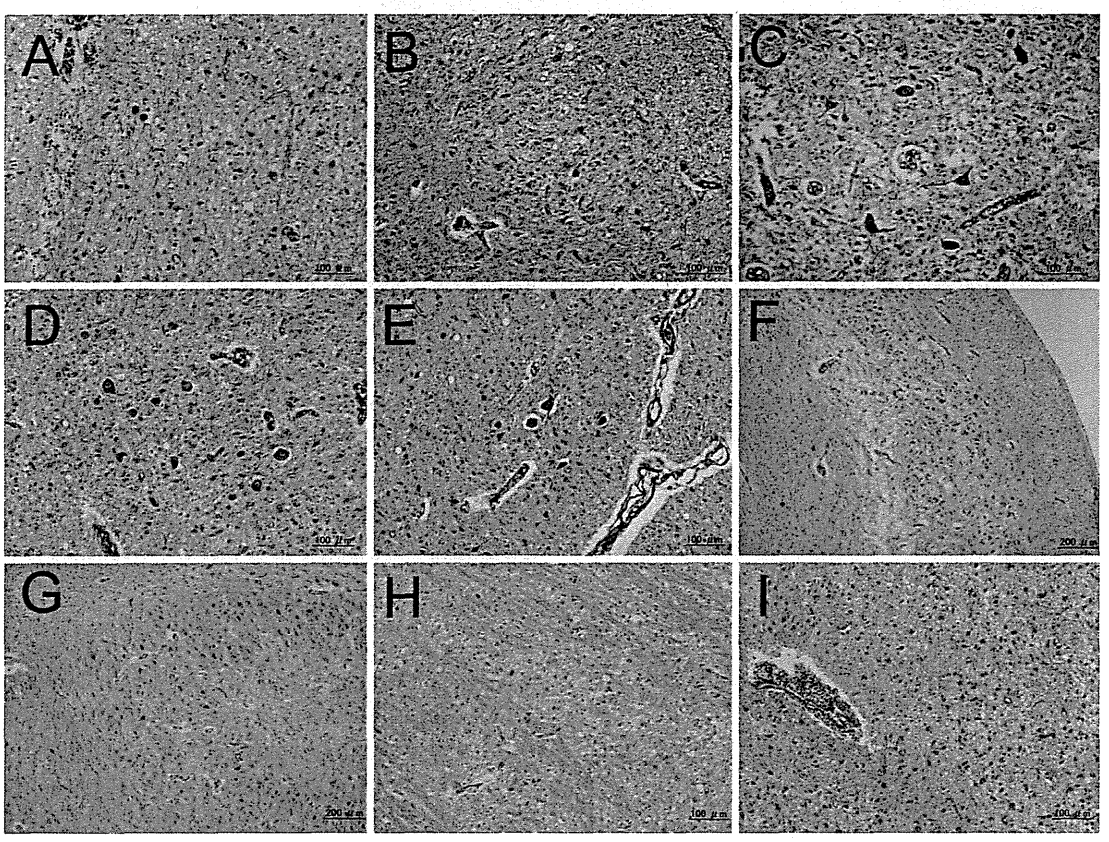

Figure 3. Neuronal loss and gliosis in the lower motor neuron nuclei: severe in the oculomotor (III) (A) and hypoglossal (XII) (B) nuclei; moderate in the motor nuclei of the trigeminal (V) (C) and facial (VII) nerves (D); and mild in the nucleus ambiguus (E). In the hippocampus, CA1-2 and the subiculum (F) are relatively preserved. However, severe neuronal loss and gliosis are evident in CA3-4 (G). Moderate neuronal loss is observed in the putamen (H) and thalamus (I).

nuclei; moderate in the motor nuclei of the trigeminal (V) and facial (VII) nerves; and mild in the nucleus ambiguus], hippocampus (severe in CA3-4, relatively preserved in CA1-2 and the subiculum), parahippocampal gyrus (moderate), amygdala (severe in the medial part), caudate nucleus (moderate), putamen (moderate), thalamus (moderate), brainstem reticular formation including the raphe nucleus (severe), gracile and cuneate nuclei (severe), inferior olivary nucleus (severe), and spinal gray matter (severe in the anterior horn, relatively preserved in the posterior horn and intermediolateral nucleus) (Fig. 3, Fig. 4B, and Table). There was diffuse myelin pallor in the cerebral white matter. Diffuse myelin pallor with macrophage infiltration was also evident in the brainstem (central tegmental tract and medial leminiscus) and spinal cord (Fig. 4A). There was patchy myelin pallor in both spinal anterior and posterior nerve roots (Fig. 4C).

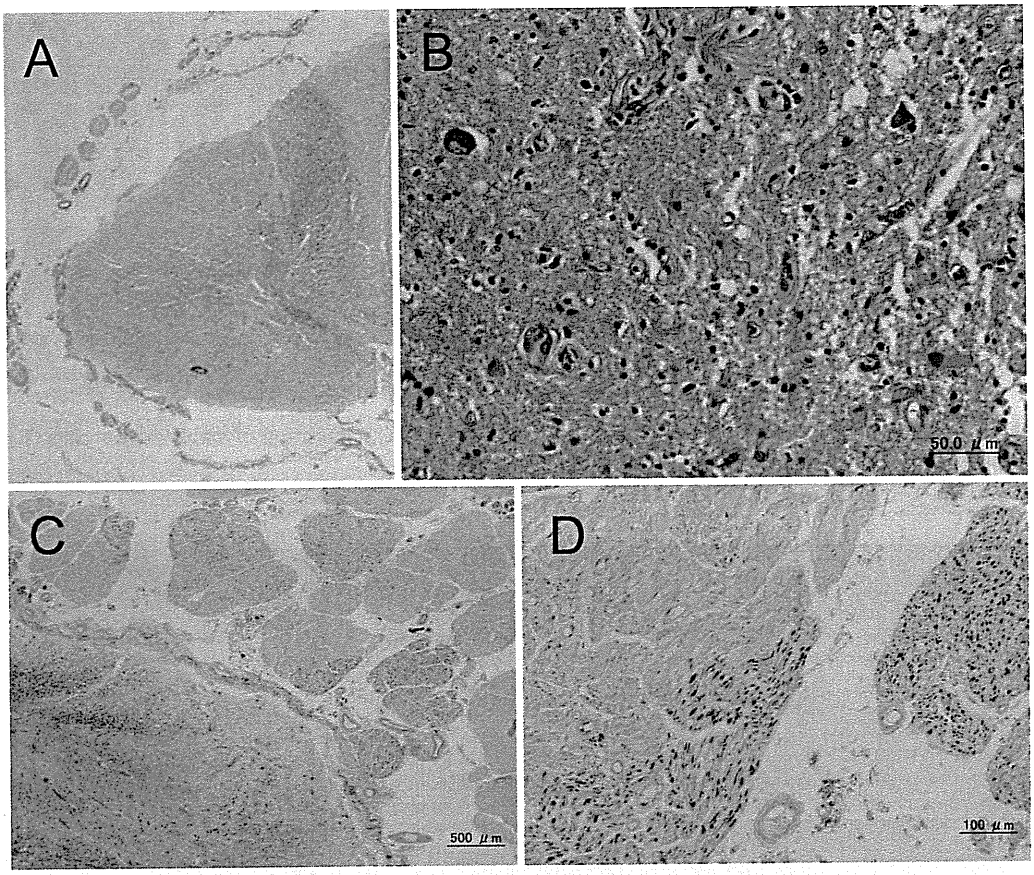

Figure 4. Diffuse myelin pallor is evident in the spinal white matter, including the lateral corticospinal tract (A). Severe neuronal loss and gliosis is evident in the lumbar anterior horn (B). Myelin pallor is evident in the nerve roots (C). SMI-31 immunostaining demonstrates patchy loss of myelinated axons (D).

Table. Degree of Neuronal Loss in the Central Nervous System

Degree of neuronal loss	Site
Severe	occulomotor nuclei, hypoglossal nuclei, hippocampus (CA3-4), amygdala, raphe nucleus, gracile and cuneate nuclei, inferior olivary nucleus, anterior horn, Purkinje cell
Moderate	nuclei of the trigeminal and facial nerve , hippocampus (CA1-2 and subiculum), parahippocampal gyrus, caudate nucleus, putamen, thalamus, posterior horn and intermediolateral nucleus, cerebellar dentate nucleus
Mild	nucleus ambiguus

Immunostaining with SMI31, a marker for axon, also showed patchy axonal damage (Fig. 4D). Purkinje cell loss and Bergmann's gliosis were evident in the cortex, being more marked in the superior part of the vermis. The cerebellar dentate nucleus was relatively well preserved. Occasional perivascular and intraparenchymal lymphocytic infiltration was seen throughout the entire affected regions. A few microglial nodule- and neuronophagia-like lesions were also seen in the affected brainstem and spinal gray matter.

Discussion

The present case was characteristic in its combination of symptoms of mental deterioration, upper and lower motor neuron disturbance, and various autonomic system failures with rapid progression. Extensive work-up for the origin of the malignancy was negative, and an autopsy first revealed the esophageal SCC. We concluded that the neurological deficit was caused by a paraneoplastic etiology because there was no tumor invasion in the nervous system. Moreover, since anti-Hu antibody was detected in her serum, this patient was diagnosed with anti-Hu syndrome.

The autopsy examination showed severe disintegration in the major part of the brain in the present patient. It was difficult to determine whether the damage originated from the hypoxia due to the pneumonia or the anti-Hu syndrome. Despite the softness of the brain, global ischemia or hypoxia could be excluded because the vulnerable regions for hypoxia including the basal ganglia, Ammon's horn, tegmentum, substantia nigra, and calcarine, were relatively preserved microscopically. Moreover, whole layer involvement, not laminar necrosis, was evident throughout the entire cortex. These findings suggested that the broad damage of the